Redox Biology 74 (2024) 103225

Contents lists available at ScienceDirect

Redox Biology

journal homepage: www.elsevier.com/locate/redox

FAM3A plays a key role in protecting against tubular cell pyroptosis and acute kidney injury

Xiaolong Li [a,1], Feifei Yuan [a,1], Yabing Xiong [a,1], Ying Tang [b,1], Zhiru Li [a], Jun Ai [a], Jinhua Miao [a], Wenting Ye [a], Shan Zhou [a], Qinyu Wu [a], Xiaoxu Wang [a], Dan Xu [a], Jiemei Li [a], Jiewu Huang [a], Qiurong Chen [a], Weiwei Shen [a], Youhua Liu [a], Fan Fan Hou [a], Lili Zhou [a,*]

[a] State Key Laboratory of Organ Failure Research, National Clinical Research Center of Kidney Disease, Guangdong Provincial Clinical Research Center for Kidney Disease, Guangdong Provincial Key Laboratory of Nephrology, Division of Nephrology, Nanfang Hospital, Southern Medical University, Guangzhou, China
[b] Department of Nephrology, The Third Affiliated Hospital of Southern Medical University, Guangzhou, China

ARTICLE INFO

Keywords:
AKI
Pyroptosis
Mitochondria
FAM3A
NRF2

ABSTRACT

Acute kidney injury (AKI) is in high prevalence worldwide but with no therapeutic strategies. Programmed cell death in tubular epithelial cells has been reported to accelerate a variety of AKI, but the major pathways and underlying mechanisms are not defined. Herein, we identified that pyroptosis was responsible for AKI progression and related to ATP depletion in renal tubular cells. We found that FAM3A, a mitochondrial protein that assists ATP synthesis, was decreased and negatively correlated with tubular cell injury and pyroptosis in both mice and patients with AKI. Knockout of FAM3A worsened kidney function decline, increased macrophage and neutrophil cell infiltration, and facilitated tubular cell pyroptosis in ischemia/reperfusion injury model. Conversely, FAM3A overexpression alleviated tubular cell pyroptosis, and inhibited kidney injury in ischemic AKI. Mechanistically, FAM3A promoted PI3K/AKT/NRF2 signaling, thus blocking mitochondrial reactive oxygen species (mt-ROS) accumulation. NLRP3 inflammasome sensed the overload of mt-ROS and then activated Caspase-1, which cleaved GSDMD, pro-IL-1β, and pro-IL-18 into their mature forms to mediate pyroptosis. Of interest, NRF2 activator alleviated the pro-pyroptotic effects of FAM3A depletion, whereas the deletion of NRF2 blocked the anti-pyroptotic function of FAM3A. Thus, our study provides new mechanisms for AKI progression and demonstrates that FAM3A is a potential therapeutic target for treating AKI.

1. Introduction

Over 13 million patients are suffering acute kidney injury (AKI) each year, and AKI is with a high mortality up to 23 % [1–3]. As one of the main reasons of chronic kidney disease (CKD) and end-stage renal disease (ESRD), AKI not only brings a threat to individual health but also imposes a high cost to social economy. However, except for supportive therapies, no treatment strategies for AKI are available nowadays [3]. Thus, finding new strategies of AKI prevention is of great value to all nephrologists.

Programmed cell deaths primarily include apoptosis, necroptosis, ferroptosis, pyroptosis, and others. In AKI progression, tubular epithelial cells could undergo one or multiple forms of cell death to contribute a variety of pathological changes [4]. Recently, cell pyroptosis, characterized by cell swelling and highly triggering inflammation, is an especial form of tubular cell death in AKI [5]. Pyroptosis is driven by the activation of endogenous danger or stress responses-stimulated NLRP3/ASC inflammasome [6]. After that, Caspase-1 is recruited and activated to subsequently induce proteolysis of interleukin-1β (IL-1β) and interleukin-18 (IL-18) and the transformation into their mature forms. Moreover, activated Caspase-1 cleaves Gasdermin-D (GSDMD) to generate N-terminal fragment (GSDMD-N) to trigger transmembrane pores formation. Active IL-1β and IL-18 are then released and along with GSDMD-N to strongly promote inflammation, cell swelling, and cell destruction [7]. Of note, NLRP3 inflammasome activation, inflammation, and cell destruction are also the typical characteristics of AKI [5,8,9], suggesting the existence of cell pyroptosis in AKI. However, this should be clarified in detail.

* Corresponding author.
E-mail address: jinli730@smu.edu.cn (L. Zhou).
[1] These authors contribute equally to this work: Xiaolong Li, Feifei Yuan, Yabing Xiong, Ying Tang.

https://doi.org/10.1016/j.redox.2024.103225
Received 28 February 2024; Received in revised form 21 May 2024; Accepted 4 June 2024
Available online 8 June 2024

Mitochondrion is the central organelle to produce adenosine 5′-triphosphate (ATP) for energy supply. Mitochondrial dysfunction not only leads to the decrease in ATP production, but also triggers the production of mitochondrial reactive oxygen species (mt-ROS). The high production of mt-ROS has been indicated as an important mediator of AKI progression [10,11]. Notably, mt-ROS is also a strong inducer to cell pyroptosis, suggesting cell pyroptosis could be an important pathogenesis in AKI. However, their relationships are poorly understood.

FAM3 family is a novel cytokine-like gene family including four members like FAM3A, FAM3B, FAM3C, and FAM3D [12]. Among them, FAM3A is a new identified mitochondrial protein that interacts with F1-ATP synthase to enhance ATP generation [13]. Recent reports have shown that FAM3A deficiency could reduce ATP production in

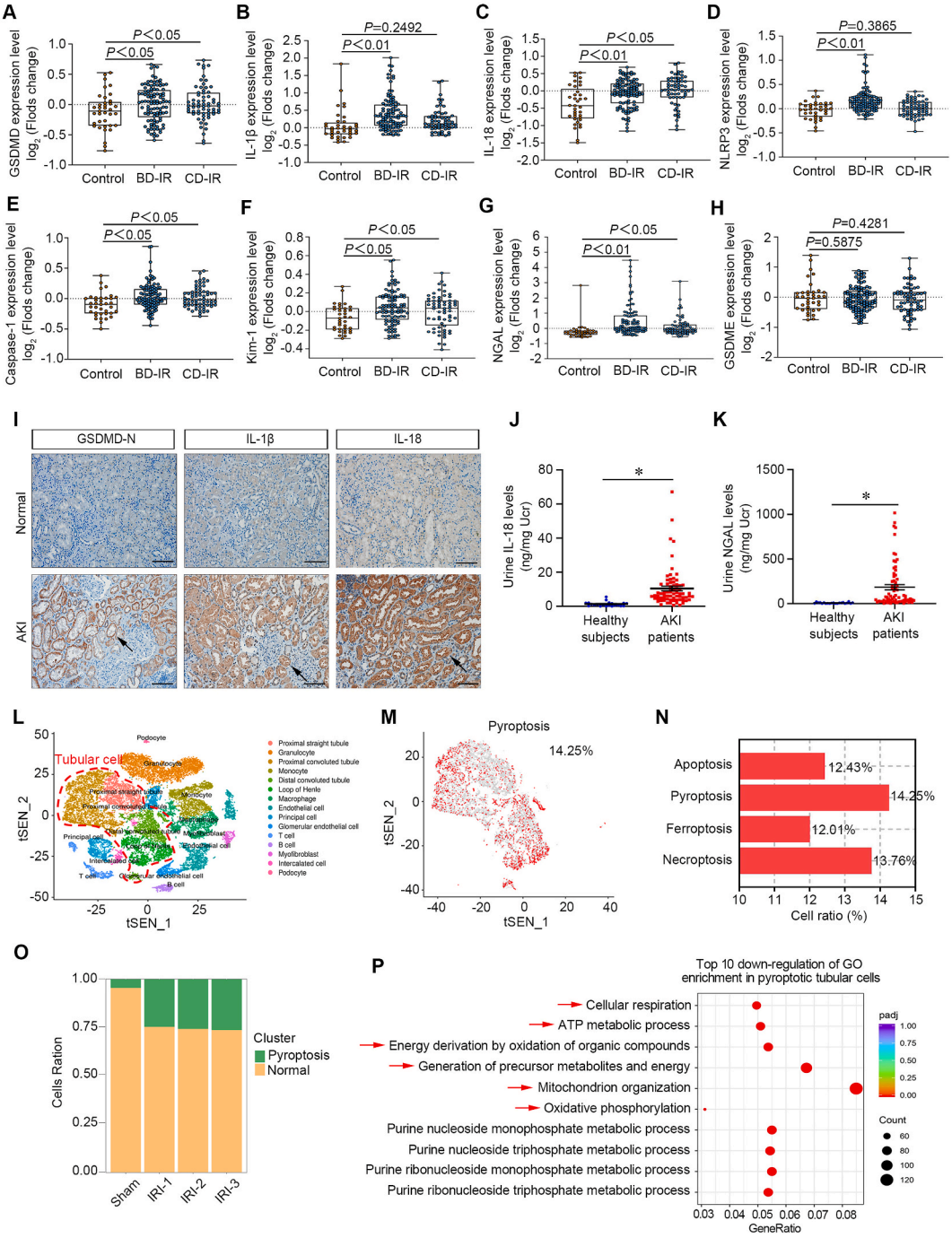

Fig. 1. Tubular cell pyroptosis is critical to AKI progression and highly related to energy production barrier. (A–H) The relative levels of GSDMD, IL-1β, IL-18, NLRP3, Caspase-1, Kim-1, NGAL, and GSDME in kidneys from different groups as indicated. n = 37 controls, n = 105 BD-IR, n = 64 CD-IR. (I) Representative micrographs show immunohistochemical staining of GSDMD-N, IL-1β, and IL-18 in kidneys from normal and AKI patients. Arrows indicate positive staining. Scale bar, 50 μm. (J–K) The levels of IL-18 and NGAL in urine from healthy subjects and AKI patients. *$P < 0.05$ versus healthy subjects. n = 21 healthy subjects, n = 71 AKI patients. (L) tSNEs show cell population in kidneys of sham and IRI at 1,2, and 3 days. The range of red broken line presents tubular cells. Total cell numbers, 33,518. Tubular cells numbers, 14,150. (M) tSENs show the pyroptotic tubular cells. (N) Graphic presentation shows the proportion of apoptotic, pyroptotic, ferroptotic, and necroptotic tubular cells. (O) Cells ratio of pyroptotic tubular cells in different groups as indicated. (P) Go enrichment shows the top 10 down-regulated BP (biological process) pathways in pyroptotic tubular cells compared to the normal. Arrows denote mitochondria ATP synthesis-related pathways.

hepatocytes, smooth muscle cells, and endothelial cells [14–16]. Furthermore, ATP binds with P2 receptor to induce PI3K/AKT pathway activation (so-called ATP signaling) [12,14]. Recent studies found FAM3A is highly involved in hepatic steatosis, liver ischemia/reperfusion injury, brain impairment, and vascular remodeling [14,17–19], however, its role in kidney diseases has not been reported. As a mitochondrial protein, FAM3A possibly plays a key role in tubular cell homeostasis and highly involved in AKI. However, this should be thoroughly investigated.

In this study, we identified that pyroptosis is an important form of tubular cell death in AKI. FAM3A was significantly decreased in AKI, and intimately correlated with kidney function preservation. FAM3A was a promising protector against renal tubular cell pyroptosis and AKI by activating PI3K/AKT/NRF2 pathway. Our findings provide a new mechanism for the pathogenesis of AKI and propose a promising therapeutic strategy for treating AKI.

2. Results

2.1. Tubular cell pyroptosis is critical to AKI progression, and is related to mitochondrial dysfunction

We first analyzed transcriptomics data of human ischemia-reperfusion (IR)-affected kidneys, including BD-IR (brain-dead IR kidneys) or CD-IR (cardiac-dead IR kidneys), from published dataset [20] to assess the expression of pyroptosis-related genes and tubular injury markers. As shown, the pyroptotic genes such as GSDMD, NLRP3, Caspase-1, IL-18, and IL-1β, as well as tubular injury markers NGAL and Kim-1, were increased in IR (Fig. 1A–G). However, GSDME, another important Gasdermin protein member, showed no significant changes in IR kidneys (Fig. 1H), suggesting that GSDMD could play a critical role in AKI. The staining also showed in clinical AKI patients, GSDMD-N, IL-1β, and IL-18 were significantly increased when compared with healthy control (Fig. 1I). We also found urinary IL-18 level was increased in AKI patients, accompanied by the elevation of NGAL, β2-MG, and UACR (Fig. 1J–K and Figs. S1A–B), indicating the intimate association of pyroptosis with tubular injury.

Furthermore, cell death was evaluated in murine AKI model using single-cell RNA-seq dataset [1,21]. We extracted tubular epithelial cells, including proximal straight tubule, proximal convoluted tubule, loop of Henle, and distal convoluted tubule (Fig. 1L). According to different lists of programmed cell death markers, we identified the percentage of tubular cells undergoing apoptosis, pyroptosis, ferroptosis, and necroptosis, was 12.43 %, 14.25 %, 12.01 %, and 13.76 %, respectively (Fig. 1M − N and Figs. S1C–E), suggesting tubular cell pyroptosis is the major form of death in AKI. However, the cell viability of cultured tubular cells under treating with hypoxia/reoxygenation (H/R), could be improved by applying pyroptosis, ferroptosis, apoptosis, and necroptosis inhibitors, suggesting that all forms of tubular cell death contribute to the progression of AKI (Fig. S1F). Notably, cell pyroptosis happened at an early stage and continuously remained at a high level following AKI progression (Fig. 1O and S1G-I). Gene ontology (GO) enrichment analysis revealed that in these pyroptotic tubular cells, ATP metabolic process, cellular respiration, mitochondrion organization, and others are greatly downregulated (Fig. 1P), suggesting pyroptosis is highly related to energy production obstacles. However, the underlying mechanisms need to be further explored.

2.2. Mitochondrial FAM3A is decreased in AKI and associated with tubular epithelial cell pyroptosis

Through analyzing sc-RNA-seq data, we found that FAM3A was downregulated in all segments of tubules in AKI (Fig. S1J). Furthermore, the correlation network analysis showed that FAM3A was highly correlated with cell pyroptosis, cellular carbohydrate metabolic process, etc. In addition, the sc-RNA-seq analysis revealed that its downregulation was most pronounced in pyroptotic tubular cells (Fig. 2A–B). To induce pyroptosis, TNF-α and NLRP3 activators were administered into cultured tubular cells. NLRP3 and GSDMD-N levels were upregulated and this indicated the cell pyroptosis (Fig. 2C and Fig. S1K-L). In addition, FAM3A was downregulated accompanied by reduced TOMM20, a mitochondrial mass marker (Fig. 2C–D and Fig. S1M − N). Co-staining of FAM3A and tubular segment-specific markers showed that FAM3A was expressed in all segments of tubules in health control mice (Fig. 2E). We also isolated mitochondria and found FAM3A was located in mitochondria and was strongly decreased after IRI (Fig. 2F–G). Furthermore, we performed double staining of FAM3A with TOMM20. As shown in Fig. 2H, FAM3A was downregulated in those tubules with decreased TOMM20. To further identify the expression of FAM3A in tubules in AKI, we isolated primary renal tubules from IRI mice at different time points (6h, 24h, 48h, 7day). As shown, FAM3A expression was decreased at an early stage (6h) in AKI mice, and maintained decreasing following AKI progression (Fig. 2I). In IRI-affected kidneys, FAM3A was greatly decreased, and accompanied by the increase in GSDMD-N (Fig. 2J,K and Fig. S1P). Immunostaining showed GSDMD-N was highly increased in AKI mice. The decrease in FAM3A in AKI was also testified by qPCR (Fig. S1Q). We also found that the downregulation of FAM3A was likely pronounced in the proximal tubules rather than the distal tubules (Fig. S1O).

The downregulation of FAM3A was also demonstrated in patients with AKI, both by staining in kidney biopsy and by analysis of RNA-seq data (Fig. 2L-M). Of interest, co-staining showed the tubules with lower expression of FAM3A had strong expression of GSDMD-N (Fig. 2N). Furthermore, urinary FAM3A excretion was significantly increased in AKI (Fig. 2O-P and Fig. S1R), and importantly, it was positively correlated with IL-18, NGAL, and β2-MG levels in urine from AKI patients (Fig. 2Q–S). These findings indicate repressed FAM3A plays a key role in AKI and is associated with tubular cell pyroptosis.

2.3. Gene ablation of FAM3A aggravates kidney injury in IRI model

To investigate the role of FAM3A in AKI, we constructed tubular cell-specific FAM3A knockout mice ($FAM3A^{CKO}$). The successful gene ablation in proximal tubules was confirmed by PCR, immunostaining, and immunoblotting (Fig. 3A–E, F-G). Sex- and age-matched WT and $FAM3A^{CKO}$ mice were used to construct ischemic AKI model and the experiment design was shown in Fig. 3B. Expectedly, serum creatinine and BUN were significantly upregulated in IRI mice. However, these indexes were further increased in IRI-affected $FAM3A^{CKO}$ mice, indicating that FAM3A depletion worsens AKI (Fig. 3C–D). Consistently, the results of immunoblotting or immunostaining showed the tubular injury markers NGAL and Kim-1 were further elevated, while the epithelial marker E-cadherin and mitochondrial marker TOMM20 were further lost in $FAM3A^{CKO}$ mice after IRI surgery (Fig. 3F, H-J, and Figs. S2A–B). The PAS staining also showed the injury tubules were further increased in IRI-affected $FAM3A^{CKO}$ mice (Fig. 3J–K). Notably, the expression of P2Y1, a purinergic P2 receptor, was reduced in WT mice after IRI surgery and further downregulated due to gene ablation of tubular FAM3A, suggesting that the ATP signaling inhibition could be the major cause to mediate FAM3A depletion-aggravated AKI (Fig. S2C). Moreover, gene ablation of FAM3A exacerbated the infiltration of inflammatory cells such as $F4/80^{+}$ macrophages and $Ly6G^{+}$ neutrophils (Fig. 3L-N). We also found renal function and morphological features of nephrons were normal after tubular FAM3A knockout in WT mice. These results indicated that gene deletion of FAM3A worsens AKI through inhibiting ATP signaling and facilitating inflammation.

2.4. Knockout of FAM3A aggravates tubular cell pyroptosis via suppressing PI3K/AKT/NRF2 pathway

To further evaluate the mechanism by which FAM3A deletion aggravates AKI, RNA sequencing was performed in IRI-affected WT and

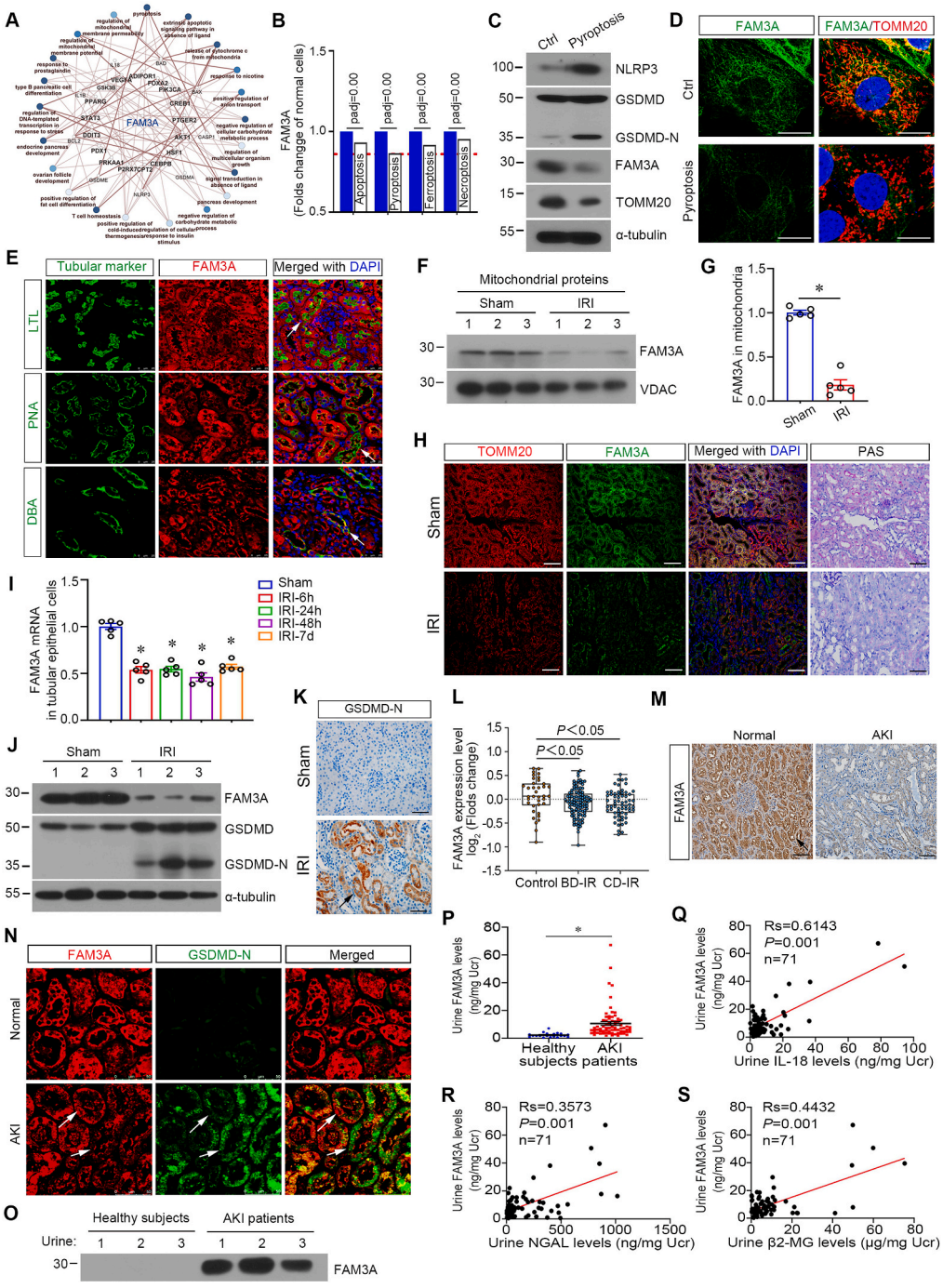

Fig. 2. Mitochondrial FAM3A is downregulated and associated with tubular cell pyroptosis in AKI. (A) Network analysis of FAM3A-related genes in biological process enrichment. (B) The expression of FAM3A in normal, apoptotic, pyroptotic, ferroptotic, and necroptotic tubular cells. Broken line denotes the level of FAM3A in pyroptotic tubular cells. (C) Representative Western blot shows the protein levels of NLRP3, GSDMD, GSDMD-N, TOMM20, and FAM3A. (D) Representative micrographs show immunofluorescent co-staining of FAM3A and TOMM20 in normal and pyroptotic HKC-8 cell. Scale bar, 10 μm. (E) Representative micrographs show immunofluorescent co-staining of FAM3A with different tubular segment markers, LTL (proximal tubule), PNA (distal tubule), and DBA (collecting duct) in mouse kidney. Arrows indicate co-staining area. Scale bar, 50 μm. (F) Western blot analyses show the expression of FAM3A in the mitochondria of sham and IRI kidneys. (G) Quantitative determination of FAM3A levels in the mitochondria of sham and IRI kidneys (normalized by VDAC). $^*P < 0.05$ versus Sham (n = 5). (H) Representative images of TOMM20 and FAM3A immunofluorescent staining and PAS in normal and IRI kidneys. Scale bar, 50 μm. (I) Graphic presentation shows the relative FAM3A mRNA level in different groups as indicated. $^*P < 0.05$ versus Sham (n = 5). (J) Western blot shows the level of FAM3A and GSDMD-N in sham and IRI kidneys. (K) Representative images of GSDMD-N immunohistochemical staining in normal and IRI kidneys. Arrow indicates the positive staining. Scale bar, 50 μm. (L) The relative levels of FAM3A in kidneys from different groups as indicated. n = 37 controls, n = 105 BD-IR, n = 64 CD-IR. (M) Representative micrographs show immunohistochemical staining of FAM3A in kidneys from normal and AKI patients. Arrow indicates positive staining. Scale bar, 50 μm. (N) Immunofluorescent staining of kidney sections show the location of FAM3A and GSDMD-N. Arrows indicate the interlace colocalization of FAM3A and GSDMD-N in tubules. Scale bar, 50 μm. (O) Representative western blotting shows the protein levels of FAM3A in urines from healthy and AKI patients. (P) Graphic presentation shows the level of FAM3A in urine from healthy subjects and AKI patients. $^*P < 0.05$ versus healthy subjects. n = 21 healthy subjects, n = 71 AKI patients. (Q–S) The positive correlation between FAM3A levels and IL-18, NGAL, and β2-MG levels in AKI urine.

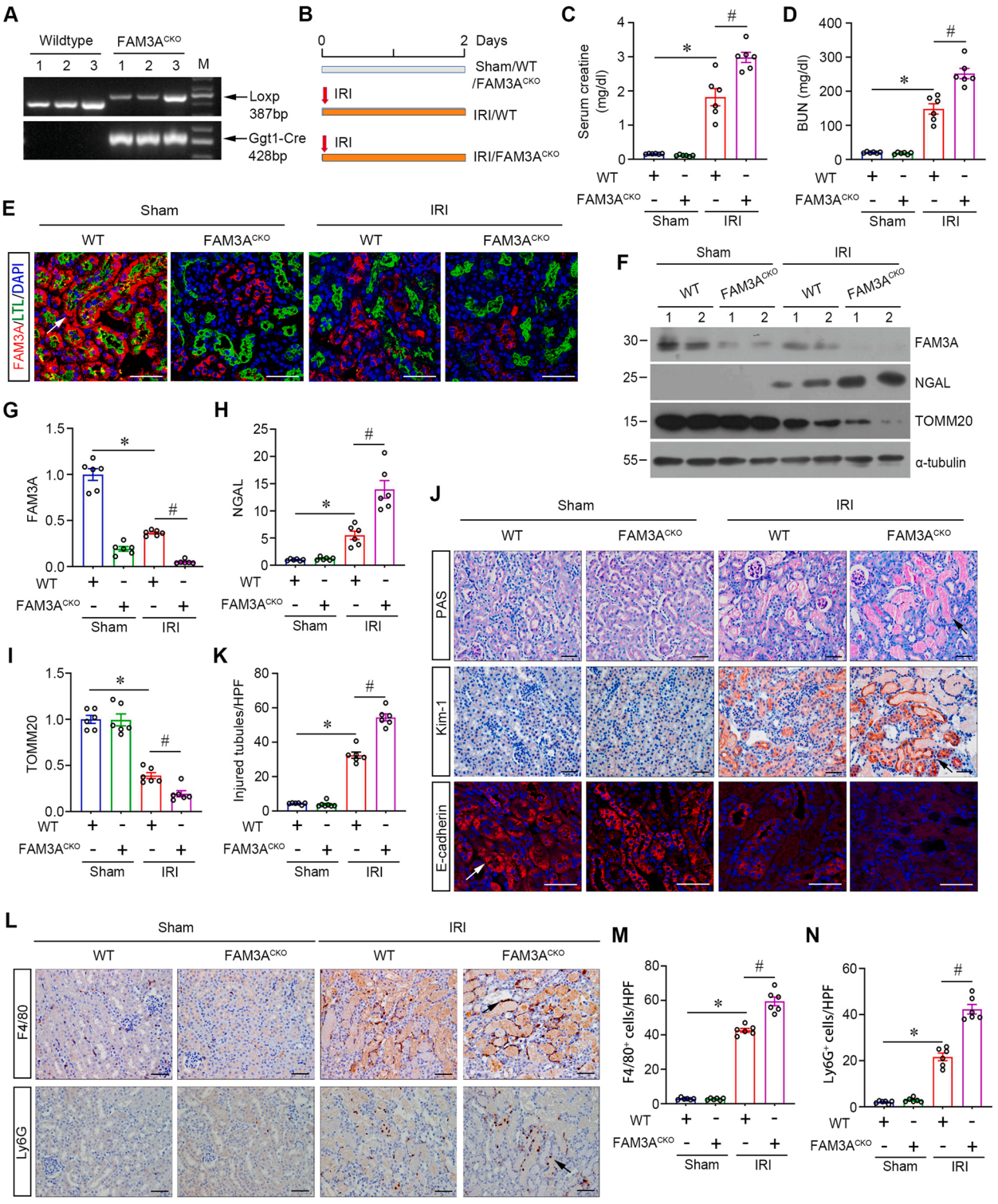

Fig. 3. FAM3A deficiency exacerbates ischemic kidney injury. (A) Mice were genotyped by using specific primers for FAM3A^{flox} and ggt1-cre. Mice carrying both FAM3A^{flox} and ggt1-cre were considered FAM3A^{CKO}. (B) Experimental design of ischemic AKI model in different groups of mice. Red arrows indicate the time points undergoing IRI. (C–D) Serum creatinine and BUN level in different groups as indicated. *$P < 0.05$ versus WT controls, #$P < 0.05$ versus WT-IRI mice (n = 6). (E) Representative micrographs show immunofluorescent co-staining of FAM3A with LTL in kidneys from different groups. Arrow indicates positive staining. Scale bar, 50 μm. (F) Representative Western blot shows the protein levels of FAM3A, TOMM20, and NGAL. (G–I) Graphic presentation shows FAM3A, TOMM20, and NGAL protein levels in different groups. *$P < 0.05$ versus WT controls, #$P < 0.05$ versus WT-IRI mice (n = 6). (J) Representative images of PAS, immunofluorescent and immunohistochemical staining show injured tubules, Kim-1, and E-cadherin abundance in different groups. Arrows indicate the injured tubules or the positive staining. Scale bar, 50 μm. (K) Quantitative determination of injured tubules ratio per high power field (HPF) in different groups. *$P < 0.05$ versus WT controls, #$P < 0.05$ versus WT-IRI mice (n = 6). (L) Representative images of kidney sections show immunohistochemical staining for the macrophage marker F4/80, or neutrophile marker Ly6G. Arrows indicate the positive cells. Scale bar, 50 μm. (M – N) Quantitation of F4/80$^+$ and Ly6G$^+$ cells per HPF. *$P < 0.05$ versus WT controls, #$P < 0.05$ versus WT-IRI group (n = 6).

FAM3A^{CKO} mice. 223 genes showed significant changes in FAM3A^{CKO} mice when compared with WT mice after IRI (Fig. S3A). GO enrichment exhibited knockout of FAM3A inhibited the biological processes of tubular cells in response to oxidative stress, fatty acid metabolism, etc., while the KEGG enrichment showed that inflammatory signaling and NOD-like receptor signaling pathway were up-regulated in FAM3A^{CKO} mice (Fig. S3B–C). Moreover, heatmap and gene set enrichment analysis (GSEA) suggested that FAM3A depletion suppressed PI3K-AKT signaling pathway, NRF2-regulated genes, and importantly induced pyroptosis (Fig. 4A–B, Figs. S3D–F). Subsequently, the abundance of p-PI3K, *p*-AKT, *p*-NRF2, and pyroptosis-related genes in tubules were detected by immunostaining and immunoblotting. As shown in Fig. 4C–D, the levels of p-PI3K, *p*-AKT, and *p*-NRF2 were mainly increased in tubules from IRI mice. However, these phosphorylated proteins were significantly reduced in tubules of FAM3A^{CKO} mice (Fig. S3G–I). Furthermore, we performed the staining of FAM3A, p-PI3K, *p*-AKT, and *p*-NRF2 on sequential kidney sections from IRI-affected FAM3A^{CKO} mice. As shown, along with the deficiency of FAM3DA, PI3K/AKT/NRF2 pathway was also inhibited (Fig. S3J). Moreover, the expression of NRF2-regulated genes Nqo1 and Sod1 was suppressed, and the accumulation of mt-ROS was promoted in IRI-affected FAM3A^{CKO} mice (Fig. 4E–H). Importantly, knockout of FAM3A further elevated the upregulation and activation of NLRP3, Caspase-1, IL-1β, IL-18, and GSDMD in IRI mice (Fig. 4H–J, and Fig. S4A–G). The staining on sequential sections showed in the same tubules, decreased FAM3A induced the upregulation of NLRP3 and GSDMD-N (Fig. 4I). Interestingly, we also assessed GSDME and found it was not changed after knockout of tubular FAM3A in AKI (Fig. S4H–I). These findings demonstrated that knockout of FAM3A facilitates tubular cell pyroptosis via inhibiting PI3K/AKT/NRF2 pathway.

2.5. Overexpression of FAM3A protects against AKI and alleviates tubular cell pyroptosis through promoting PI3K/AKT/NRF2 pathway

FAM3A was overexpressed by intravenous injection of FAM3A expression plasmid (pFAM3A) through a hydrodynamic-based gene delivery approach 2 days before IRI surgery (Fig. 5A). Overexpression of FAM3A was verified by immunoblotting and immunostaining (Fig. 5B–E). In contrast to the findings in FAM3A^{CKO} mice, FAM3A overexpression inhibited the downregulation of P2Y1 and the increase in serum creatinine and BUN after IRI (Fig. 5F–H). PAS staining and Kim-1 immunostaining showed injury tubules increased in IRI mice, but were decreased by FAM3A overexpression (Fig. 5I–K). Consistently, E-cadherin and TOMM20 were decreased, and NGAL was increased in IRI mice but they were blocked by FAM3A overexpression (Fig. 5I, andL-O). Furthermore, F4/80 and Ly6G staining showed macrophages and neutrophils were massively aggregated in IRI, but they were greatly decreased by ectopic FAM3A (Fig. 5P-R).

Mechanistically, overexpression of FAM3A promoted the activation of PI3K, AKT, and NRF2 in tubules in IRI mice (Fig. 6A–F). We then performed the staining of FAM3A, p-PI3K, *p*-AKT, and *p*-NRF2 on sequential sections from IRI mice with ectopic expression of FAM3A. As shown, in FAM3A-positive tubules, p-PI3K, *p*-AKT, and *p*-NRF2 were also strongly induced (Fig. 6C). Furthermore, IRI-induced mt-ROS production (Fig. 6G–H) and the activation of NLRP3, Caspase-1, GSDMD, IL-1β, and IL-18, could be downregulated by overexpression of FAM3A (Fig. 6I-N). Similar results were observed in the immunohistochemical staining of GSDMD-N and NLRP3 (Fig. 6O and Fig. S5). We also performed the staining of FAM3A, NLRP3 and GSDMD-N on sequential sections from FAM3A-overexpressed IRI mice. As shown, in FAM3A-positive tubules, NLRP3 and GSDMD-N were greatly inhibited (Fig. 6P). These results further clarified that FAM3A protects against AKI and inhibits tubular cell pyroptosis through PI3K/AKT/NRF2 signaling.

2.6. Knockdown of FAM3A aggravates tubular cell pyroptosis in vitro

In vitro experiments, the human proximal tubular epithelial cell line HKC-8 cells were cultured and treated with H/R or cisplatin. As shown in Fig. 7A, FAM3A was downregulated after H/R stimulation. To assess the role of FAM3A in tubular cells, siRNA was transfected into HKC-8 to knock down FAM3A expression (Fig. S6A–C). We also found that knockdown of FAM3A further reduced ATP production in cells after treating H/R (Fig. 7B). To assess the role of FAM3A in tubular cell death, cell viability and, LDH release, a cell death marker, were then tested. As shown, H/R-decreased cell viability was aggravated by knockdown of FAM3A. Interestingly, this phenomenon was reversed by adoption of pyroptotic inhibitors Ac-YVAD-cmk and Disulfiram, rather than inhibitors of ferroptosis, apoptosis, and necroptosis (Fig. 7C and D). Importantly, knockdown of FAM3A mainly promoted the expression of genes associated with pyroptosis although also induced others to some extent (Fig. S6D). Furthermore, pyroptosis-related proteins NLRP3, Caspase-1, IL-18, IL-1β, and GSDMD were further exacerbated by knockdown of FAM3A (Fig. 7E and Fig. S6E–I). However, the activation of GSDME was not changed after knockdown of FAM3A (Fig. S6J–K). Scanning electron microscope (SEM) images showed that small protrusion bodies were formed on the cell surface after H/R stimulation, and these phenomena were more prominent in FAM3A-interffered cells (Fig. 7F). Consistently, we also found that the loss of cell viability and LDH release in cisplatin-treated cells were also aggravated by knockdown of FAM3A, but this was inhibited by pyroptotic inhibitor rather than others (Fig. S7A–B). Moreover, the activation of NLRP3, Caspase-1, IL-18, IL-1β, and GSDMD were further increased by knockdown of FAM3A in cells treating with cisplatin (Fig. S7C–H). There is also no change in GSDME activation in cisplatin-treated cells with indifference of FAM3A Fig. S7I–J. The facilitation of FAM3A knockdown in cisplatin-induced tubular cell pyroptosis was also detected by SEM (Fig. S7K).

Mechanistically, knockdown of FAM3A suppressed the activation of PI3K and AKT and reduced the accumulation of NRF2 in the nucleus (Fig. 7G–J and Fig. S8A–D). Importantly, the production of mt-ROS was further triggered by knockdown of FAM3A in H/R or cisplatin-stimulated cells (Fig. 7K-L and Fig. S8E–F). HKC-8 cells were then pretreated with AKT activator SC79, or NRF2 activator Olipraz. As shown, knockdown of FAM3A aggravated LDH release, but this was significantly inhibited by co-treatment with SC79 or Olipraz (Fig. 7M and Fig. S8G). Furthermore, knockdown of FAM3A increased GSDMD-N expression, but this was also blocked by addition of SC79 or Olipraz (Fig. 7N-O and Figs. S8H–I). To demonstrate that whether knockdown of FAM3A suppressed PI3K/AKT/NRF2 via ATP pathway, HKC-8 cells were pretreated with ADP. The results showed that treatment with ADP could improve cell pyroptosis and increase PI3K/AKT/NRF2 activation in FAM3A-interffered HKC-8 cells during H/R stimulation (Fig. 7P and Fig. S8J-M). These findings further demonstrated that FAM3A protects against cell pyroptosis through PI3K/AKT/NRF2 pathway.

2.7. NRF2 ablation eliminates the inhibitory of effects of FAM3A in cell pyroptosis

To investigate the important role of NRF2 in FAM3A pathway, primary tubular cells were isolated from NRF2 knockout mice (NRF2^{KO}) or wild-type mice (Fig. 8A–B, Fig. S9A). In WT primary tubular cells, FAM3A expressing plasmid (pFAM3A) or empty vector (pcDNA) was transfected into cells. After overexpression of FAM3A, the phosphorylation of PI3K, AKT, NRF2, and ATP production, were all increased (Fig. 8C–H). However, this pathway was suppressed after treatment with neutralizing antibody to P2Y1 (Fig. S9B–E). Notably, ectopic FAM3A inhibited H/R-increased LDH production in WT primary tubular cells, but not in NRF2^{KO} primary tubular cells (Fig. 8I). H/R induced very pronounced characteristics of cell pyroptosis in WT primary tubular cells, but overexpression of FAM3A inhibited it. Howevere, this could not be seen in NRF2^{KO} primary tubular cells (Fig. 8J). In addition, the beneficial effects of FAM3A in reducing mt-ROS were blocked when NRF2 was knocked out (Fig. 8J–K). Importantly, overexpression of FAM3A repressed the activation of NLRP3, Caspase-1, IL-18, IL-1β, and

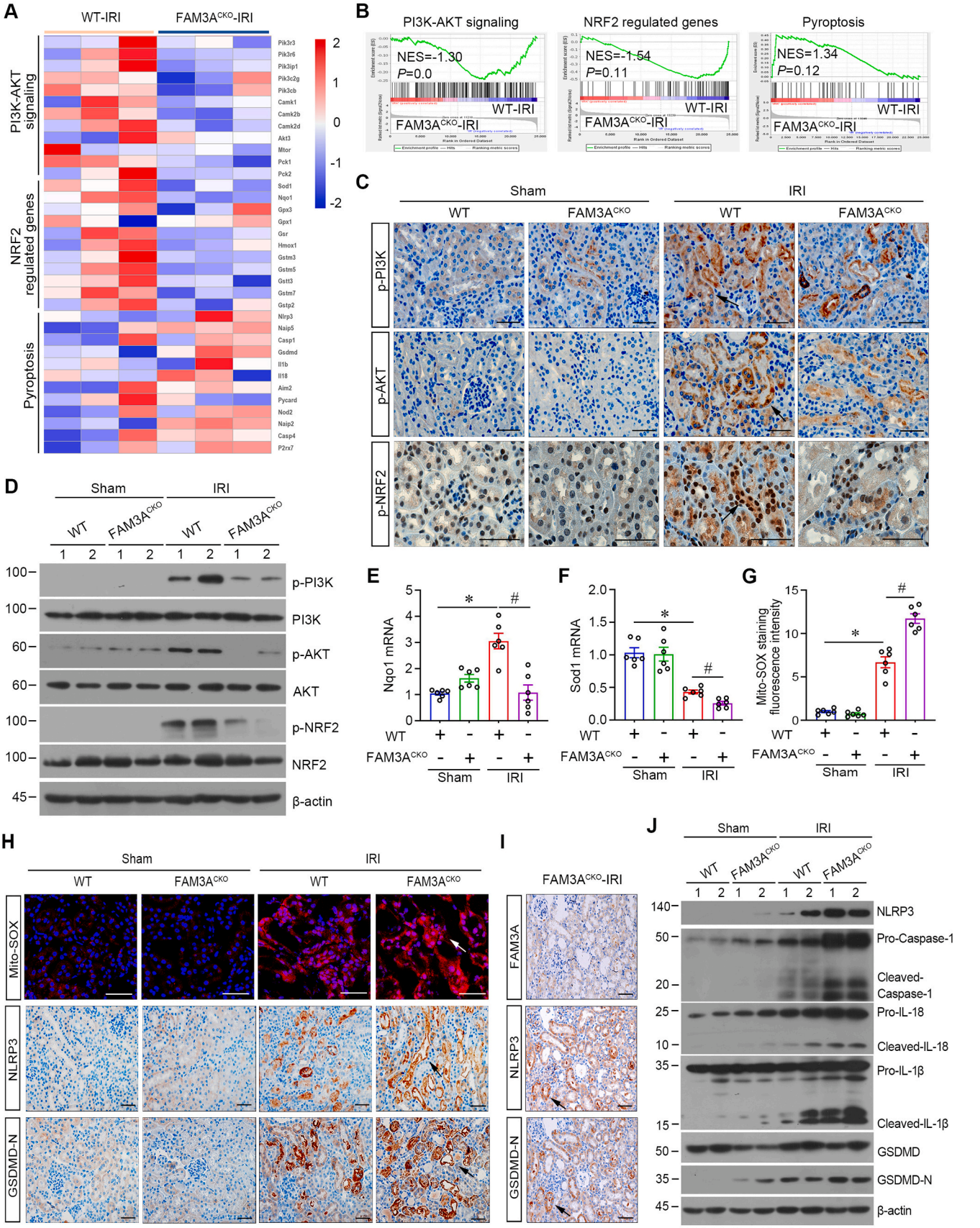

(caption on next page)

Fig. 4. FAM3A deficiency promotes pyroptosis by suppressing PI3K/AKT/NRF2 pathway. (A) The heatmap shows PI3K-AKT signaling, NRF2 regulated genes, and pyroptosis in WT and FAM3A^{CKO} mice in IRI (n = 3 per group). (B) GSEA shows that the decreased PI3K-AKT signaling and NRF2-regulated genes enrichment, and increased pyroptosis in FAM3A^{CKO} mice compared with WT mice. (C) Representative micrographs show the abundance of p-PI3K, *p*-AKT, and *p*-NRF2. Arrows indicate positive staining. Scale bar, 20 μm. (D) Representative Western blot shows the protein levels of p-PI3K, PI3K, *p*-AKT, AKT, *p*-NRF2, and NRF2 in different groups as indicated. (E–F) qPCR analyses show the expression of Nqo1 and Sod1 in the kidneys from different groups as indicated. $^{*}P < 0.05$ versus WT controls, $^{\#}P < 0.05$ versus WT-IRI mice (n = 6). (G) Quantitation of Mito-SOX fluorescence intensity in different groups. $^{*}P < 0.05$ versus WT controls, $^{\#}P < 0.05$ versus WT-IRI mice (n = 6). (H) Representative images of Mito-SOX staining and immunohistochemical staining of GSDMD-N and NLRP3. Arrows indicate positive staining. Scale bar, 50 μm. (I) Representative micrographs show the expression of FAM3A, NLRP3 and GSDMD-N on the sequential kidney sections from IRI-affected FAM3A^{CKO} mice. Arrows indicate positive staining. Scale bar, 50 μm. (J) Representative western blotting shows the protein levels of renal NLRP3, Pro-caspase-1, Cleaved-caspase-1, Pro-IL-18, Cleaved-IL-18, Pro-IL-1β, Cleaved-IL-1β, GSDMD, and GSDMD-N in different groups as indicated.

GSDMD in H/R-stimulated WT cells, but not in NRF2 knockout cells (Fig. 8L-R). These results suggest that NRF2 plays a key role in FAM3A pathway.

2.8. Activation of NRF2 ameliorates cell pyroptosis in IRI-FAM3A^{CKO} mice

We further assessed whether treatment with NRF2 activator could alleviate tubular epithelial cell pyroptosis in IRI-FAM3A^{CKO} mice. We treated these mice with a natural compound of NRF activator, sulforaphane (SFN) (Fig. 9A). NRF2 was activated and its downstream targets Nqo1 and Sod1 were both upregulated by SFN (Fig. 9B–F). Of note, mt-ROS accumulation was suppressed by co-treatment with SFN (Fig. 9G–H). Of interest, cell pyroptosis-related proteins NLRP3, Caspase-1, IL-18, IL-1β, and GSDMD-N were all further activated in IRI-affected FAM3A^{CKO} mice, but these were blocked by co-treatment with SFN (Fig. 9I-N). Similar results were observed when GSDMD-N and NLRP3 were examined by immunohistochemistry (Fig. 9O-Q).

Importantly, FAM3A ablation aggravated the increase in serum creatine and BUN levels in IRI mice, while co-treatment with SFN significantly decreased them (Fig. 10A–B). Co-treatment with SFN could also significantly alleviate tubular injury, decreased NGAL and Kim-1 expression, and inhibited macrophage and neutrophil infiltration in IRI-affected FAM3A^{CKO} mice (Fig. 10C–I). Hence, as the schematic representation (Fig. 10J), we found FAM3A is an important target for treating AKI, which participates in ATP synthesis and secretion in tubular epithelial cells. Through inducing P2Y1/PI3K/AKT/NRF2 pathway, FAM3A plays a key role in protecting against tubular cell pyroptosis and AKI.

3. Discussion

The numbers of patients with AKI are greatly increasing. AKI is facing no effective therapeutic strategies and unclear mechanisms [3,4]. Renal tubular cells are major components of kidney parenchyma and are vulnerable to multiple injuries. They could undergo a variety of transformation processes such as proliferation, epithelial-mesenchymal transitions, cell cycle arrest, vacuolar degeneration, and even cell death [22–24]. Of note, tubular cell death is the most important cause of rapid progression of AKI disease, which could trigger cast formation to induce oliguria or anuria. Understanding the underlying mechanisms of tubular cell death is of great value in clarifying the pathogenesis of AKI and finding new effective therapeutic strategies.

Our study demonstrates that tubular cell pyroptosis is an important form of programmed cell death in AKI and reveals that impairment of mitochondrial energy production may be a critical mechanism. Especially, mitochondrial FAM3A is reduced in tubular epithelial cells in AKI, and is associated with tubular cell pyroptosis. FAM3A deficiency in proximal tubules worsens, whereas FAM3A overexpression protects against pyroptosis in AKI. The PI3K/AKT/NRF2 axis is a downstream signaling of FAM3A, which assists in mt-ROS clearance via regulating antioxidative gene expression. However, FAM3A is deficient in AKI, which suppresses PI3K/AKT/NRF2 signaling axis, thus limiting mt-ROS clearance and ultimately evoking pyroptosis (Fig. 10J)

Tubular cell death could present multiple forms, such as apoptosis, ferroptosis, pyroptosis, and necroptosis, which all participate in AKI [4]. Even if apoptosis is considered an important tubular cell death form in AKI, however, inhibition of apoptosis has been reported no effects to ameliorate AKI, suggesting that another type of cell death may be primarily responsible for disease progression [25,26]. Among multiple forms of cell death, ferroptosis and pyroptosis were found to primarily participate in the progression of AKI in recent study [1]. However, which one is more important has not been elucidated. In this study, we performed single-cell sequencing data analysis and found that pyroptosis-positive tubular epithelial cells occupied the highest proportion in ischemic kidneys. Our study innovatively uncovers the most important contribution of tubular epithelial cell pyroptosis in AKI. Consistently, a previous report has shown that knockout pyroptosis-associated genes, such as NLRP3, Caspase-1, Caspase-11, and GSDMD, could improve kidney function in cisplatin or contrast-induced AKI [27,28]. However, the underlying mechanisms of cell pyroptosis in tubular cells have not been clarified.

From our results, GO enrichment reveals that mitochondrial energy production was impaired in the pyroptotic tubular cells. To date, the mechanism of mitochondrial dysfunction facilitating pyroptosis has been mainly focused on mt-ROS [10,29,30], but how reduced ATP synthesis itself promotes pyroptosis remains unclear. Our present study observed that the mitochondrial protein FAM3A was dramatically reduced in pyroptotic tubular cells during IRI. FAM3A is located in the mitochondrial matrix and inner membrane and interacts with F1-ATP synthase to regulate its activity [13]. It has been observed that FAM3A deficiency reduces ATP production and secretion in hepatocytes, smooth muscle cells, endothelial cells and so on [14–16]. The role of FAM3A in kidney remains to be demonstrated in detail. Although previous findings in neuronal cells and chondrocytes have shown that FAM3A attenuates apoptosis [31,32]. Combined with bioinformatics analysis, clinical research, and in vivo and in vitro studies, the present data reveal that FAM3A was negatively associated with tubular cell pyroptosis in AKI, but not so relevant with apoptosis, ferroptosis, or necroptosis. The discrepancy may be due to the distinct pathological conditions or different types of cells. Actually, the role of energy stress with excessive ATP depletion in regulating the forms of programmed cell death is controversial. For example, it has been reported that long-term or severe energy stress in tumor cells eventually induces apoptosis [33,34]. However, glucose starvation in mouse embryonic fibroblasts inhibits ferroptosis by activating AMPK [35]. Additionally, Berry et al. observed that disrupting mitochondrial oxygen consumption and suppressing ATP generation in $CD4^{+}$ T cells ultimately triggered pyroptosis [36]. This finding is supportive to our results to implicate that the loss of FAM3A in proximal tubular cells reduced ATP generation and then facilitated pyroptosis in AKI.

It is interesting to find that FAM3A levels were elevated in urine from AKI patients. FAM3A is primarily localized in mitochondria, but it has been reported that it could be secreted by myogenic cells [37]. Despite its high expression in normal kidney and strong secretory capacity of proximal tubules, FAM3A was undetectable in the urine of healthy volunteers, suggesting that FAM3A is unlikely to be secreted by tubular cells. Notably, renal tubular cell detachment and loss are hallmarks of the pathology of AKI. Therefore, the injured tubular cells could fall into the urine, which triggers the strong induction of FAM3A in urine.

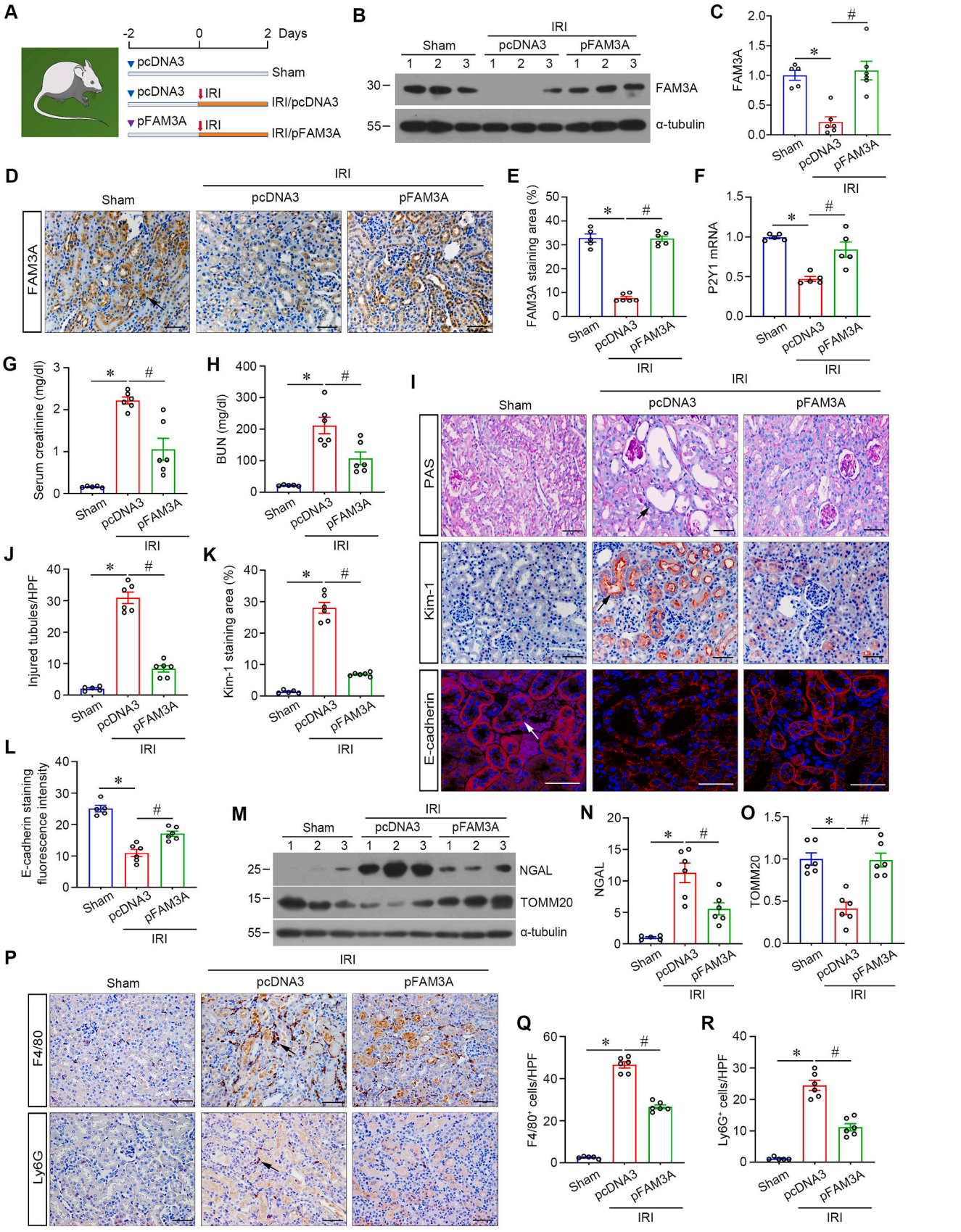

(caption on next page)

Fig. 5. Overexpression of FAM3A improves AKI. (A) Experimental design. Triangles denote the time points of pcDNA3 or pFAM3A injection. Red arrows indicate the time points undergoing IRI. (B) Representative Western blot shows the protein level of FAM3A in different groups as indicated. (C) Quantitative determination of FAM3A expression in different groups. *$P < 0.05$ versus controls, #$P < 0.05$ versus pcDNA3-IRI mice (n = 5–6). (D) Representative image of FAM3A immunohistochemical staining. Arrows indicate positive staining. Scale bar, 50 μm. (E) Quantitation of FAM3A staining area in different groups. *$P < 0.05$ versus controls, #$P < 0.05$ versus pcDNA3-IRI mice (n = 5–6). (F) qPCR analyses show the expression of P2Y1 in the kidneys from different groups as indicated. *$P < 0.05$ versus controls, #$P < 0.05$ versus pcDNA3-IRI mice (n = 5). (G–H) Serum creatinine and BUN level in different groups as indicated. *$P < 0.05$ versus controls, #$P < 0.05$ versus pcDNA3-IRI mice (n = 5–6). (I) Representative images of PAS, immunofluorescent and immunohistochemical staining show injured tubules, Kim-1, and E-cadherin expression in different groups. Arrows indicate the injured tubules or the positive staining. Scale bar, 50 μm. (J–L) Quantitation of injured tubules ratio (HPF), Kim-1 staining positive area, and E-cadherin staining fluorescence intensity of kidneys from different groups. *$P < 0.05$ versus controls, #$P < 0.05$ versus pcDNA3-IRI mice (n = 5–6). (M) Representative Western blot shows the protein levels of NGAL and TOMM20. (N–O) Graphic presentation shows the relative NGAL and TOMM20 protein abundance in different groups as indicated. *$P < 0.05$ versus controls, #$P < 0.05$ versus pcDNA3-IRI mice (n = 5–6). (P) Representative micrographs of immunohistochemical staining for the macrophage marker F4/80, or neutrophile marker Ly6G. Arrows indicate the positive staining. Scale bar, 50 μm. (Q–R) Quantitation of the number of $F4/80^+$ and $Ly6G^+$ cells per HPF. *$P < 0.05$ versus controls, #$P < 0.05$ versus pcDNA3-IRI mice (n = 5–6).

Furthermore, we also tested the correlation between urinary FAM3A and NGAL, a marker for tubular cell injury, and found they were intimately correlated. All these suggest urinary FAM3A primarily originates from injured tubular cells. However, it is difficult to isolate the falling cells from urine, and further to identify the cell death condition in these cells because of the urine flushing, changes in mechanical stress, etc. Hence, it is very difficult to demonstrate urinary FAM3A exactly does come from pyroptotic tubular cells or other dead cell types. However, urinary FAM3A was positively correlated with urinary IL-18, a marker of cell pyroptosis, and multiple results in this study suggest that loss of FAM3A in tubules strongly mediates cell pyroptosis during AKI.

ATP-P2 receptor axis mediated FAM3A function in various tissues or cells [14,15]. Two distinct P2 receptors, P2X and P2Y receptors, mediate such actions. P2X receptor is a ligand-gated ion channel that is permeable to cations, while P2Y receptor is a G-protein-coupled receptor that stimulates PLC/IP_3 to activate downstream pathway of PI3K/AKT. It has been reported that P2Y receptors, including P2Y1, P2Y2, P2Y4, and P2Y6 are mainly expressed in proximal tubular cells, and it is more sensitive to ATP than P2X receptor [38]. Our present data revealed that P2Y1 was down-regulated after IRI and mediated the function of FAM3A in tubules. In AKI, FAM3A deficiency facilitates tubular cell pyroptosis through inhibiting P2Y1/PI3K/AKT pathway.

By RNA-seq analysis, we identified NRF2 as a downstream regulator of FAM3A. NRF2 is a redox-regulated transcription factor that combines with Keap1 and is located in the cytoplasm in normal conditions. Upon oxidative stress, NRF2 translocates to the nucleus and binds to the antioxidant response element (ARE), thus regulating the expression of antioxidant proteins, such as Ho1, Sod1, and Nqo1, to assist in ROS clearance [39]. The function interaction between NRF2 and PI3K/AKT pathway has been well demonstrated in various cells. Inhibition of PI3K/AKT signal reduces the nuclear accumulation of NRF2 [40,41]. Consistent with these findings, the present study reveals that when knockout of FAM3A suppressed PI3K/AKT activation, the nuclear translocation of NRF2 was inhibited in tubules after injury, resulting in increased mt-ROS accumulation. The overloaded mt-ROS eventually induces pyroptosis. Pharmacological activation of NRF2 improves the negative impacts of FAM3A deficiency on promoting tubular cell pyroptosis in AKI. Conversely, depletion of NRF2 eliminates the protective effect of FAM3A overexpression on alleviating tubular cell pyroptosis. These observations highlight the critical role of NRF2 in the protection of FAM3A against pyroptosis.

mt-ROS is a damage-associated molecular patterns (DAMPs) signal, which could be sensed by NLRP3 inflammasome to activate Caspase-1/GSDMD pathway [30]. In FAM3A-deficient tubular epithelial cells, we found the accumulation of large amounts of mt-ROS, which originates from the inhibition of NRF2 activation. Interestingly, we also found FAM3A deficiency mediated pyroptosis in AKI primarily through GSDMD-N, rather than GSDME-N, both of them are reported to drive tubular cell pyroptosis. The pyroptotic cells release various pro-inflammatory factors, such as IL-1β and IL-18, to form an inflammatory microenvironment. This could not only modulate neutrophils and macrophages infiltration but also induce more and more damage to tubular cells [5,7]. Reports have shown pro-inflammatory factors are the accelerators of pyroptosis [42], this may explain why pyroptosis maintains at a high level throughout AKI process.

Our findings also observed that the downregulated FAM3A promoted the loss of mitochondrial mass. It is well known that mitochondrion is a sensitive and brittle organelle that can be injured in various pathological conditions, such as inflammation, ROS, ischemia and hypoxia [11]. The loss of mitochondria in injured cell due to suppressed mitochondrial biogenesis facilitates mitochondrial fragmentation. Oxidative stress could aggravate mitochondrial mass loss, but FAM3A could inhibit oxidative stress by activating NRF2 signaling. Hence, FAM3A not only regulates mitochondrial respiratory function, but also affects the homeostasis of mitochondrial mass. However, this should be clarified in detail in the future.

Another important finding is we found FAM3A was a sensitive indicator for mitochondrial injury. As we know, in IRI mice or AKI patients, the hypoxia microenvironment in whole kidney would affect all types of cells, especially the tubules with huge consumption of oxygen. Based on the different extents of hypoxia microenvironment in whole kidney, cell injury would be exhibited in different extents. Hence, even if some tubules look like normal in visual, however, the hypoxia and reperfusion microenvironment would still lead to the damage of organelles with sensitive sensing ability, such as mitochondria. Interestingly, we found in those tubules not dilated, and with no loss of cells and no casts, which look like normal in morphology just under visual observation, however, their expression of TOMM20 was already decreased, suggesting the mitochondrial damage. Concomitantly, the expression of FAM3A in those tubules with loss of TOMM20, was also greatly decreased. But in PAS staining, those tubules still look like normal with no evident phenomena of dilation and casts formation. Therefore, we thought FAM3A was a sensitive indicator of tubular cell mitochondrial injury even in those tubules with no evident morphology changes yet.

In conclusion, our findings provide strong evidences that mitochondrial dysfunction contributes to AKI and associates with tubular cell pyroptosis. We also found that FAM3A represents a potential novel protective target against AKI.

4. Materials and methods

4.1. Animal models

Male C57BL/6 mice at 8–12 weeks weighting about 20–25g were supplied from the Southern Medical University Animal Center (Guangzhou, China). All mice were housed in a pathogen-free, humidity- and temperature-controlled environment and maintained with standard diet and water. The ischemic/reperfusion AKI model was built according to established protocol [43,44]. Briefly, mice were randomly divided into different groups as indicated and anesthetized with sodium pentobarbital (60 mg/ml). Subsequently, a midline abdominal incision was made and bilateral renal pedicles were clipped by microaneurysm clamps for 30 min at 37.5 °C. After 48 h, mice were sacrificed and serum and kidney tissues were collected for further analyses. In

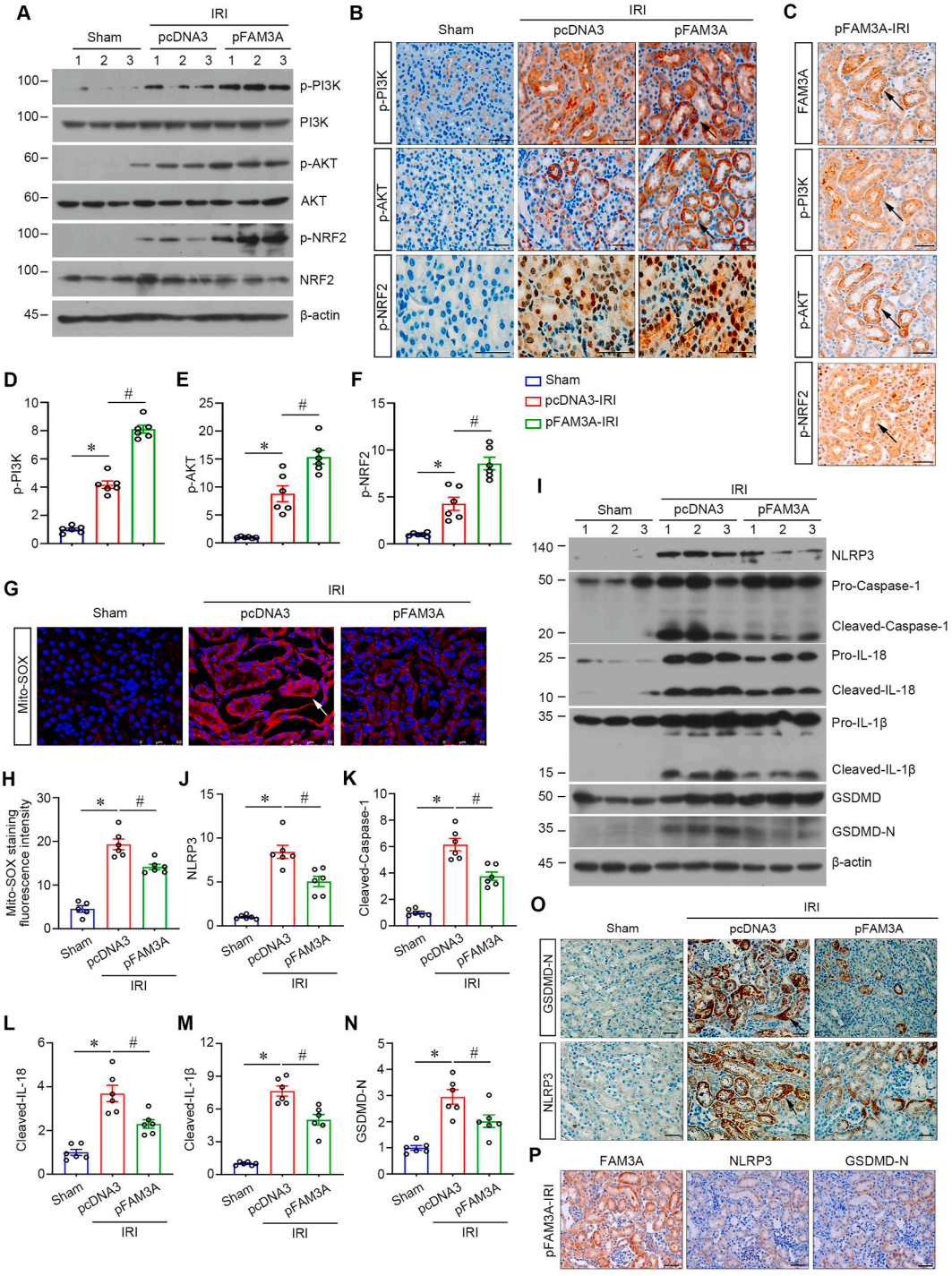

Fig. 6. FAM3A overexpression alleviates pyroptosis by activating PI3K/AKT/NRF2 signaling. (A) Representative Western blot shows the protein levels of p-PI3K, PI3K, *p*-AKT, AKT, *p*-NRF2, and NRF2 in different groups as indicated. (B) Representative micrographs show the abundance of p-PI3K, *p*-AKT, and *p*-NRF2. Arrows indicate positive staining. Scale bar, 20 μm. (C) Representative micrographs show the co-localization of FAM3A, p-PI3K, *p*-AKT, and *p*-NRF2 in renal tubules in FAM3A-overexpressed IRI mice. Arrows indicate positive staining. Scale bar, 20 μm. (D–F) Quantitative proteins expression of p-PI3K, PI3K, *p*-AKT, AKT, *p*-NRF2, and NRF2. $^{*}P < 0.05$ versus controls, $\#P < 0.05$ versus pcDNA3-IRI group (n = 6). (G) Representative images show mt-ROS levels in the kidneys of mice from different groups. Arrows indicate positive staining. Scale bar, 50 μm. (H) Quantitative determination of Mito-SOX staining fluorescence intensity in different groups. $^{*}P < 0.05$ versus controls, $\#P < 0.05$ versus pcDNA3-IRI group (n = 5–6). (I) Representative western blotting shows the protein levels of renal NLRP3, Pro-caspase-1, Cleaved-caspase-1, Pro-IL-18, Cleaved-IL-18, Pro-IL-1β, Cleaved-IL-1β, GSDMD, and GSDMD-N in different groups as indicated. (J–N) Quantitation of the protein levels of NLRP3, Cleaved-caspase-1, Cleaved-IL-18, Cleaved-IL-1β, and GSDMD-N in different groups. $^{*}P < 0.05$ versus controls, $\#P < 0.05$ versus pcDNA3-IRI group (n = 6). (O) Representative micrographs of immunohistochemical staining show the abundance of GSDMD-N and NLRP3. Arrows indicate positive staining. Scale bar, 50 μm. (P) Representative micrographs show the expression of FAM3A, NLRP3 and GSDMD-N on the sequential kidney sections from FAM3A-overexpressed IRI mice. Scale bar, 50 μm.

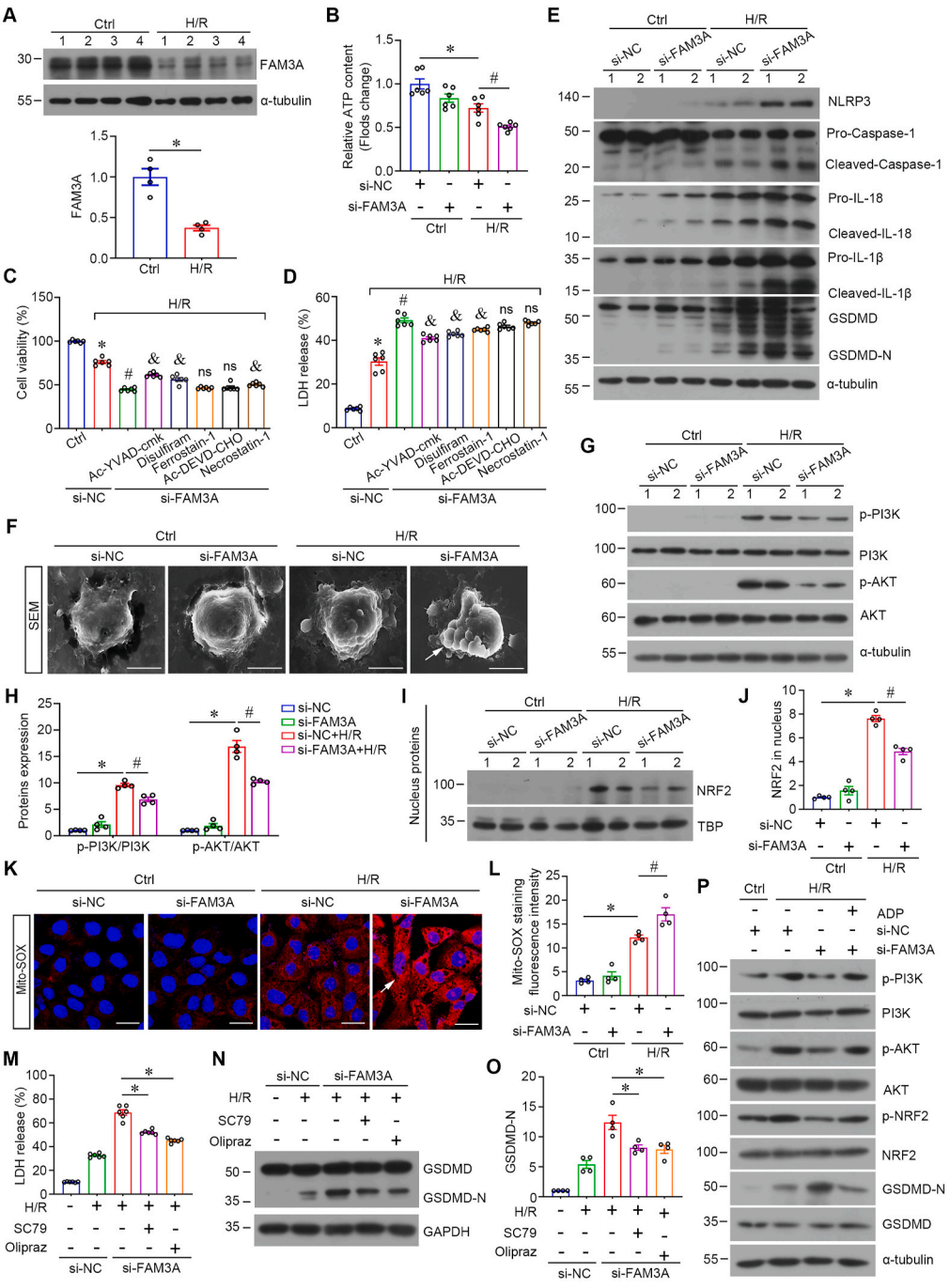

Fig. 7. Knockdown of FAM3A accelerates tubular epithelial cell injury. (A) Western blotting and quantitation show the expression of FAM3A in HKC-8 after H/R treatment. *$P < 0.05$ versus control group, (n = 4). (B) Graphic presentation shows the relative ATP content in HKC-8 from different groups as indicated. *$P < 0.05$ versus normal negative controls, #$P < 0.05$ versus the cell treatment with H/R (n = 6). (C) Graphic presentation shows the viability of cells from different groups as indicated. *$P < 0.05$ versus controls, #$P < 0.05$ versus the cell treated with si-NC and H/R, &$P < 0.05$ versus the cell treated with si-FAM3A and H/R (n = 6). ns, no significant difference. (D) Graphic presentation shows the cellular LDH release ratio in different groups as indicated. *$P < 0.05$ versus controls, #$P < 0.05$ versus the cell treated with si-NC and H/R, &$P < 0.05$ versus the cell treated with si-FAM3A and H/R (n = 6). ns, no significant difference. (E) Representative western blotting shows the protein levels of NLRP3, Pro-caspase-1, Cleaved-caspase-1, Pro-IL-18, Cleaved-IL-18, Pro-IL-1β, Cleaved-IL-1β, GSDMD, and GSDMD-N in different groups as indicated. (F) SEM images show the phenotype of pyroptosis of HKC-8 after H/R stimulation. Arrows indicate the protrusion bodies. Scale bar, 2 μm. (G) Representative Western blot shows the protein levels of p-PI3K, PI3K, *p*-AKT, and AKT in different groups as indicated. (H) Quantitation of the levels of PI3K, p-PI3K, AKT, *p*-AKT in cells stimulated with H/R. *$P < 0.05$ versus controls, #$P < 0.05$ versus the cell received si-NC and H/R (n = 4). (I) Western blot shows the accumulation of NRF2 in nucleus. (J) Graphic presentation shows the relative NRF2 protein abundance. Data were normalized by TBP. *$P < 0.05$ versus controls, #$P <$ 0.05 versus the cell received si-NC and H/R (n = 4). (K) Representative image of Mito-SOX red staining in the HKC-8 from different groups as indicated. Arrows indicate positive staining. Scale bar, 50 μm. (L) Quantitation of Mito-SOX red staining fluorescence intensity of HKC-8 from different groups as indicated. *$P < 0.05$ versus controls, #$P < 0.05$ versus the cell received si-NC and H/R (n = 4). (M) Graphic presentation shows the cellular LDH release ratio in different groups as indicated. SC79, AKT agonist. Olipraz, NRF2 agonist. *$P < 0.05$ versus the cell received si-FAM3A and H/R (n = 6). (N) Representative Western blot shows the protein levels of GSDMD and GSDMD-N. (O) Quantitation of the protein expression of GSDMD-N. *$P < 0.05$ versus the cell received si-FAM3A and H/R (n = 4). (P) Representative western blotting shows the protein levels of p-PI3K, PI3K, *p*-AKT, AKT, *p*-NRF2, NRF2, GSDMD, and GSDMD-N in different groups as indicated.

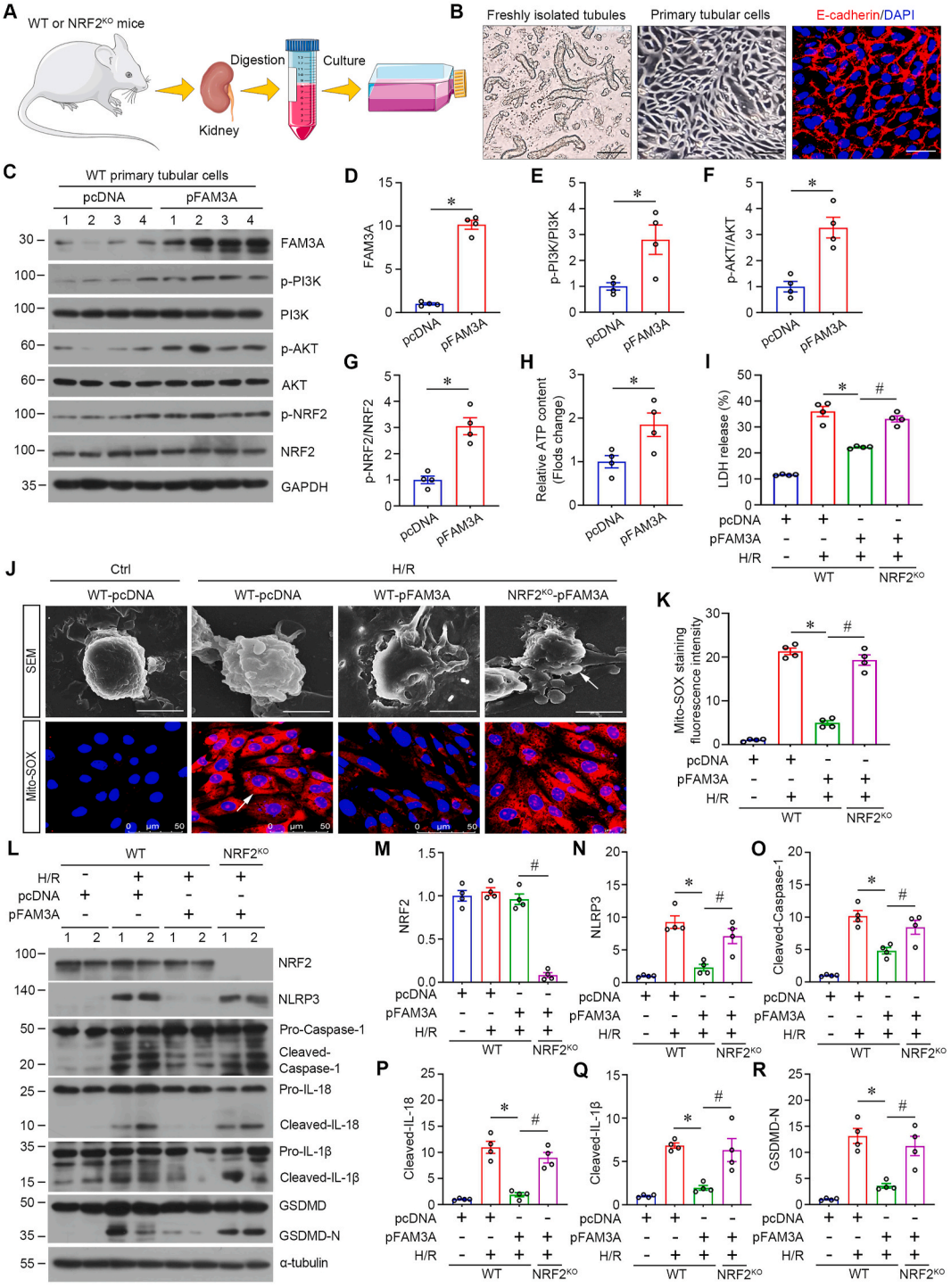

Fig. 8. The key role of NRF2 in FAM3A-alleviated **pyroptosis.** (A) The brief procedure of isolation and culture of primary tubular cells. (B) Representative micrographs exhibit freshly isolated tubules, primary tubular cells and their identified staining of E-cadherin. (C) Representative Western blot shows the expression of FAM3A, p-PI3K, PI3K, *p*-AKT, AKT, *p*-NRF2, and NRF2 in cells after transfecting with pcDNA or pFAM3A. (D–G) Quantitation of the protein levels of FAM3A, p-PI3K/PI3K, *p*-AKT/AKT, and *p*-NRF2/NRF2. *$P < 0.05$ versus pcDNA (n = 4). (H) Graphic presentation shows the relative ATP content in primary tubular cells from pcDNA or pFAM3A groups. *$P < 0.05$ versus pcDNA (n = 4). (I) Graphic presentation shows the cellular LDH release ratio in different groups. *$P < 0.05$ versus the cells received pcDNA and H/R, #$P < 0.05$ versus the cell received pFAM3A and H/R (n = 4). (J) Representative image of SEM and Mito-SOX red staining of tubular cells. Arrows indicate the protrusion bodies or positive staining. Scale bar, 2 μm (upper) or 50 μm (under). (K) Quantitative determination of Mito-SOX red staining fluorescence intensity in different groups as indicated. *$P < 0.05$ versus the cells received pcDNA and H/R, #$P < 0.05$ versus the cell received pFAM3A and H/R (n = 4). (L) Representative Western blot shows the protein levels of NRF2, NLRP3, Pro-caspase-1, Cleaved-caspase-1, Pro-IL-18, Cleaved-IL-18, Pro-IL-1β, Cleaved-IL-1β, GSDMD, and GSDMD-N in different groups as indicated. (M–R) Quantitation of the protein expression showed in (M). *$P < 0.05$ versus the cells received pcDNA and H/R, #$P < 0.05$ versus the cells received pFAM3A and H/R (n = 4).

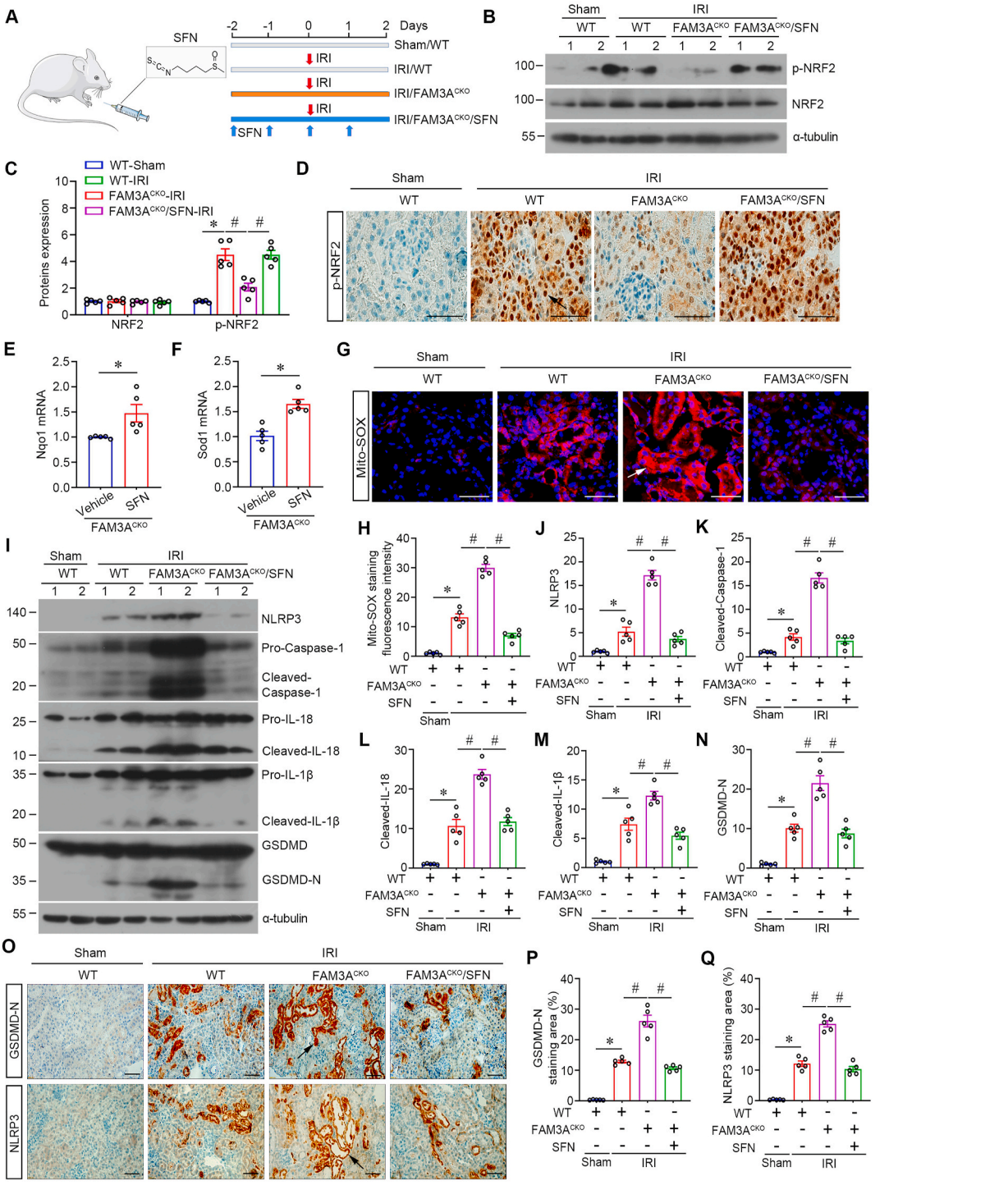

Fig. 9. NRF2 activator SFN ameliorates tubular cell pyroptosis. (A) Experiment design. SFN (10 mg/kg) was given at 2 days before IRI surgery for a continuous treatment of 4 days by intraperitoneal injection. (B) Western blot shows the levels of *p*-NRF2 and NRF2 in the kidneys from different groups as indicated. (C) Quantitation of the protein levels of NRF2 and *p*-NRF2. *$P < 0.05$ versus WT-IRI group, #$P < 0.05$ versus FAM3A^{CKO}-IRI group (n = 5). (D) Representative micrographs of *p*-NRF2 immunohistochemical staining in different groups. Arrows indicate positive staining. Scale bar, 20 μm. (E–F) qPCR showed that SFN increased NRF2-regulated genes Nqo1 and Sod1 expression. *$P < 0.05$ versus FAM3A^{CKO} mice (n = 5). (G) Representative images of Mito-SOX red staining show mt-ROS levels in the kidneys from different groups as indicated. Arrows indicate positive staining. Scale bar, 50 μm. (H) Quantitative determination of Mito-SOX staining fluorescence intensity in different groups. *$P < 0.05$ versus WT-IRI group, #$P < 0.05$ versus FAM3A^{CKO}-IRI group (n = 5). (I) Representative western blotting shows the protein levels of NLRP3, Pro-caspase-1, Cleaved-caspase-1, Pro-IL-18, Cleaved-IL-18, Pro-IL-1β, Cleaved-IL-1β, GSDMD, and GSDMD-N in different groups as indicated. (J–N) Quantitation of the protein expression showed in (I). *$P < 0.05$ versus WT-IRI group, #$P < 0.05$ versus FAM3A^{CKO}-IRI group (n = 5). (O) Representative micrographs of immunohistochemical staining show the abundance of GSDMD-N and NLRP3. Arrows indicate positive staining. Scale bar, 50 μm. (P–Q) Quantitative determination of GSDMD-N and NLRP3 staining positive area in different groups as indicated. *$P < 0.05$ versus WT-IRI group, #$P < 0.05$ versus FAM3A^{CKO}-IRI group (n = 5).

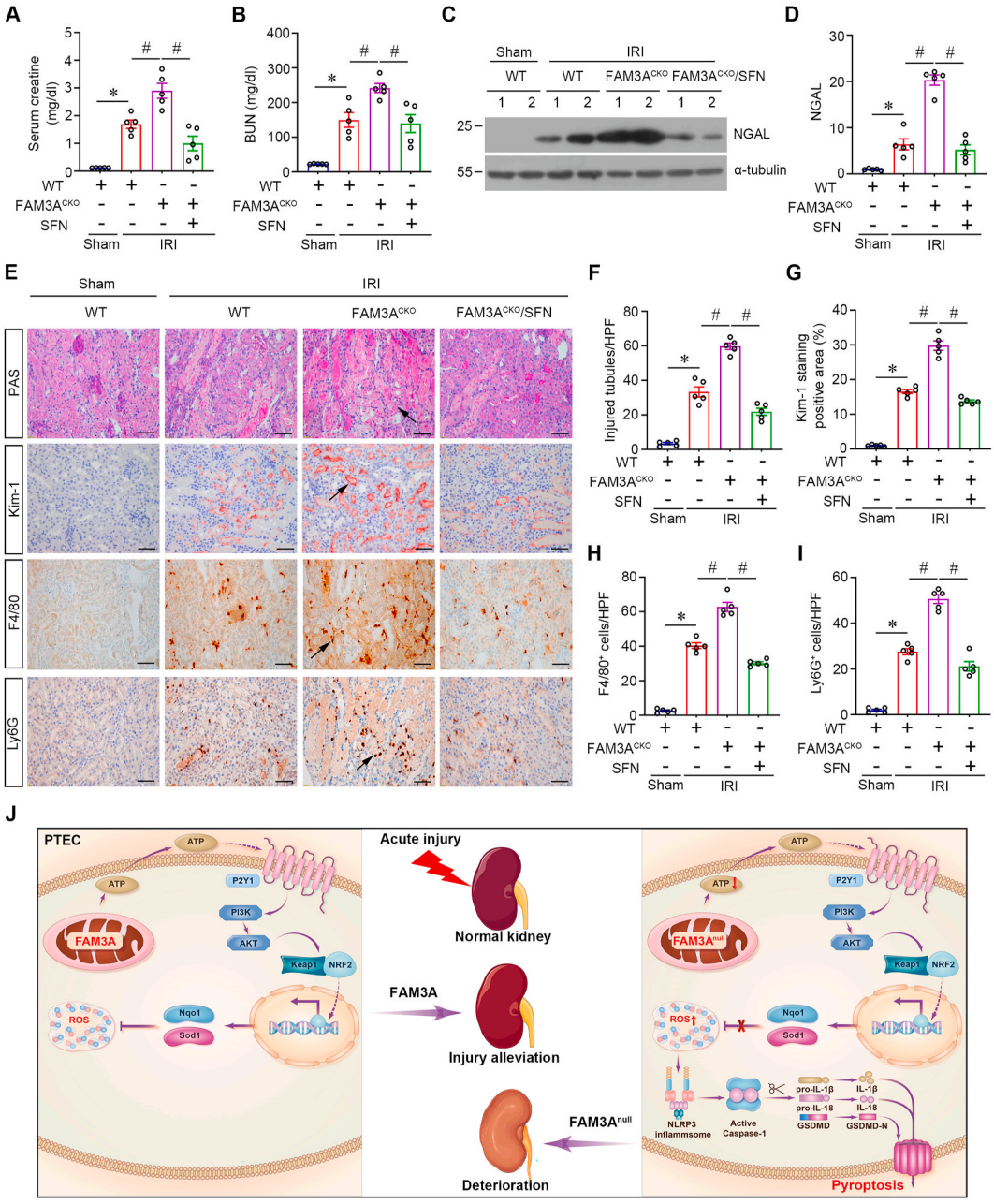

Fig. 10. Treatment with NRF2 activator improves AKI. (A–B) Serum creatinine and BUN level in different groups as indicated. *$P < 0.05$ versus WT-IRI group, #$P < 0.05$ versus FAM3A^{CKO}-IRI group (n = 5). (C) Representative Western blot shows the protein levels of NGAL. (D) Graphic presentation shows the relative NGAL protein abundance in different groups as indicated. *$P < 0.05$ versus WT-IRI group, #$P < 0.05$ versus FAM3A^{CKO}-IRI group (n = 5). (E) Representative PAS and immunohistochemical staining show injured tubules, Kim-1 expression, F4/80^{+} macrophage and Ly6G^{+} neutrophile infiltration in different groups. Arrows indicate the injured tubules or the positive staining. Scale bar, 50 μm. (F–I) Quantitative determination of injured tubules ratio per HPF, the number of F4/80^{+} and Ly6G^{+} cells per HPF. *$P < 0.05$ versus WT-IRI group, #$P < 0.05$ versus FAM3A^{CKO}-IRI group (n = 5). (J) Schematic representation of the study findings. Physiologically, mitochondrial FAM3A participates in ATP synthesis and secretion in tubular epithelial cells. Secreted ATP can activate the P2Y1/PI3K/AKT/NRF2 axis to assist mt-ROS clearance and then retard AKI. After FAM3A deficiency, the P2Y1/PI3K/AKT/NRF2 signaling axis are inhibited and the mt-ROS is accumulated. NLRP3 inflammasome senses excessive mt-ROS and then activates Caspase-1, which cleaves GSDMD, IL-1β, and IL-18, ultimately resulting in pyroptosis and worsening AKI.

pharmacological experiments, NRF2 agonist sulforaphane (SFN) was dissolved in 5 % DMSO in saline and then was administered 2 days before IRI surgery for continuous treatment of 4 days by intraperitoneal injection (10 mg/kg per day). The control mice received equal vehicle solutions.

All mice were randomly divided into different groups as indicated by using the online tool (Research Randomizer). All animal experiments were designed according to the principles of the 3Rs (Replacement, Refinement and Reduction) to minimize animal pain and reduce the number of mice used in our experiments. All animal experiments were performed in accordance with the policies of the Animal Care and Use Committee and approved by the Animal Ethic Committee at the Nanfang Hospital, Southern Medical University (Approval No. IACUC-LAC-20220713-005).

4.2. FAM3A conditional knockout mice and genotyping

Tubule-specific FAM3A knockout mice (FAM3A^{CKO}) were birthed by

mating FAM3A-floxed mice with Ggt1-cre mice, both of them were purchased from Cyagen Biosciences (Guangzhou, China). All mice were C57BL/6 N genetic background and maintained in Experimental Animal Center of Southern Medical University. The subsequent generations of mice were genotyped by PCR by using one pair of flox-specific primers and one pair of Cre-specific primers (Table S1). Age- and sex-matched $FAM3A^{CKO}$ were subjected to IRI.

4.3. NRF2 global knockout mice and genotyping

Global NRF2 knockout mice ($NRF2^{KO}$) were generated and bred by Cyagen Biosciences (Guangzhou, China). All the mice were C57BL/6 N genetic background and maintained in Experimental Animal Center of Southern Medical University. The subsequent generations of mice were genotyped by PCR by using one pair of NRF2-KO primers and one pair of WT primers (Table S1).

4.4. Overexpression of FAM3A in vivo

In vivo overexpression of FAM3A in mice was carried out by hydrodynamic-based gene delivery approach as described previously [43–45]. Briefly, the mouse FAM3A gene sequences were ligated into pcDNA3.1 plasmid. Two days before IRI, the plasmids were diluted using PBS and injected into mice via the tail vein at a dose of 2ug/g in a volume of 2 ml. The success of FAM3A overexpression was confirmed by Western blot and immunohistochemical staining.

4.5. Human kidney biopsy and urine samples

All human samples (kidney biopsy and urine) were collected from patients with AKI at the Third Affiliated Hospital of Southern Medical University following provision of written consent. The basic characteristics of AKI patients were presented in Supplementary Tables 2–3. Normal kidney tissue adjacent to tumors was collected from patients who has renal carcinoma. Healthy subjects' urines were collected from healthy volunteers. All of the experiments involving human samples were approved by the Ethic Committee on Human Subjects of the Third Affiliated Hospital of Southern Medical University (Approval No. 2023-LS-074).

4.6. Elisa

Human FAM3A Assay Kit was purchased from Raybiothech (ELH-FAM3A-1, USA), and the human IL-18 and NGAL Assay Kit was purchased from Cusabio (CSB-E07450h and CSB-E09408h, China). Human urinary FAM3A, IL-18, and NGAL were measured according to the procedures specified by the manufacturer.

4.7. Serum creatinine and BUN measurement

Serum creatinine and blood urea nitrogen (BUN) levels were determined by an automatic chemistry analyzer (AU480 Chemistry Analyzer, Beckman Coulter, Atlanta, Georgia). The levels of serum creatinine and BUN were expressed as mg/dl.

4.8. Cell culture and treatment

Human proximal tubular epithelial cells (HKC-8) were provided by Dr. Lorraine C. Racusen (Johns Hopkins University, Baltimore, MD) and cultured in DMEM/F12 containing 10%FBS at 37 °C in 5 % CO_2. To induce cell pyroptosis, TNF-α (20 ng/ml) and NLRP3 activator (10 μM, HY-139396, MCE) were added for 24h. In hypoxia/reoxygenation (H/R)-induced injury experiment, cells were incubated in glucose-free medium in a tri-gas incubator (94 % N_2, 5 % CO_2, and 1.0 % O_2) at 37 °C for 24 h. Subsequently, cells were cultured in complete medium under normal conditions for 4 h for reoxygenation. In cisplatin stimulation experiments, HKC-8 cells were first cultured in serum-free DMEM/F12 overnight and then were treated with 20 μM cisplatin for another 24h.

For knocking down or overexpression of FAM3A expression, HKC-8 cells were transfected with human FAM3A siRNA (sense: 5′- GCA-GUGGCUUUCCUCG-CAUTT-3′, antisense: 5′- AUGCGAGGAAAGCCA-CUGCTT-3′) or FAM3A plasmid, respectively, by using Lipofectamine 2000 transfection reagent (11668019, Thermo).

In pharmacological experiments, HKC-8 cells were pretreated with 10 μM PI3K/AKT activator, SC79 (HY-18749); or 10 μM NRF2 activator, Oltipraz (HY-12519); or 5 mM ADP (HY–W010918); or 5 μg/ml P2Y1 neutral antibody (APR-009, Alomone); or 10 μM Caspase-1 (pyroptosis) inhibitor, Ac-YVAD-cmk (HY-16990); or 10 μM GSDMD (pyroptosis) inhibitor, Disulfiram (HY–B0240); or 500 nM RIP kinase (necroptosis) inhibitor, Necrostain-1; or 0.23 nM Caspase-3 (apoptosis) inhibitor, Ac-DEVD-CHO (HY–P1001); or 60 nM ferroptosis inhibitor, Ferrostain-1 (HY-100579), for 1 h. All the activators and inhibitors were purchased from MCE (MedChemExpress, USA).

4.9. Isolation and culture of primary tubular epithelial cells

The isolation and culture of primary tubular epithelial cells were performed with modified procedures as previously described [44]. Briefly, the kidneys from 8 to 10 weeks old male WT or $NRF2^{KO}$ mice were minced and digested with the pre-warmed collagenase IV solution (17104-019, Gibco, USA, dissolved in serum-free DMEM/F12 medium) for 10–15min. The undigested tissue blocks were removed by a 100 μm mesh sieve. Subsequently, the renal tubules were separated on a density gradient by ultracentrifugation and the band containing predominantly proximal tubules was collected. The freshly isolated tubules were cultured in DMEM/F12 containing 10%FBS at 37 °C. After 72 h, the primary tubular epithelial cells were identified by E-cadherin immunofluorescent staining, and the following treatment was as same as that of HKC-8.

4.10. Mitochondrial isolation

Kidneys' mitochondria were collected using Tissue Mitochondria Isolation Kit (C3606, Beyotime, Shanghai, China) according to the procedures specified by the manufacturer. Firstly, fresh renal tissues were digested by trypsin-EDTA solution and then resuspended in mitochondrial isolation buffer. Secondly, the solution was centrifuged at 1000g for 10min at 4 °C to remove the nucleus and unbroken cells, the supernatant was further centrifuged at 9000g for 10min at 4 °C. After centrifuging, the supernatant was collected as cytoplasmic protein, whereas the pellet was isolated mitochondria. Finally, the isolated mitochondria were lysed with RIPA to obtain mitochondrial proteins for further experiments.

4.11. Nuclear and cytoplasmic fraction isolation

HKC-8 cells nuclear fraction was separated using nuclear protein extraction kit (BB-3102, BestBio, Shanghai, China) according to the procedures specified by the manufacturer. Briefly, HKC-8 cells were washed with cold PBS after being digested by trypsin solution. Subsequently, the solution was centrifuged at 500g for 5min at 4 °C to remove supernatant, 200 μl of cold extract A solution was added to the cell pellet, and the mixture was oscillated at 2–8 °C for 10–30 min. After mixing, the mixture was centrifuged at 2000g for 5min at 4 °C, and the 80 μl of cold extract B solution was added to the pellet and the mixture was oscillated at 2–8 °C for 30–40 min. Finally, the solution was centrifuged at 12000g for 10min at 4 °C, and the supernatant was collected as nuclear protein.

4.12. Mito-SOX staining

Kidney frozen sections and HKC-8 cells were used for detecting

mitochondrial ROS via Mito-SOX (M36008, Thermo Fisher) staining according to the manufacturer's instructions. To measure the level of tissular mito-ROS, fresh renal tissues were embedded with OCT compound (#4583, Sakura) and quickly frozen with liquid nitrogen. 3 μm kidney frozen sections were prepared and incubated with 5 μM Mito-SOX solution in dark at room temperature for 30 min. Subsequently, the sections were fixed with 4 % paraformaldehyde solution for 15 min, followed by washing with PBS, and incubated with DAPI. Finally, the images were captured by confocal microscopy and the fluorescence intensity was calculated to reflect the level of mito-ROS.

4.13. Scanning electron microscope (SEM)

The cultured cells were fixed in 1.25% glutaraldehyde/0.1 M phosphate buffer for 2h at room temperature and then saved at 4 °C. Subsequent electron microscopy embedding and photographing was performed by Huayin Medical Laboratory (Guangzhou, China).

4.14. Lactate dehydrogenase (LDH) release assay

The supernatant of HKC-8 cells was used to quantify LDH release as a measure of cytotoxicity with an LDH Cytotoxicity Assay Kit (C0016, Beyotime, China) according to the manufacturer's instructions.

4.15. Cell viability assay

After different treatments, the viability of HKC-8 cells was detected by using MTT Cell Proliferation Assay Kit (C0009S, Beyotime, China) according to the manufacturer's instructions. Briefly, the cells were incubated with 0.5 mg/ml MTT solution in dark at 37 °C for 4h. Subsequently, the cells were dissolved with DMSO and the absorbance was measured at 490 nm.

4.16. Determination of ATP content

The content of ATP of culture cells was measured with ATP Assay Kit (S0027, Beyotime, China) according to the manufacturer's instructions. ATP level was normalized by protein centration in the same sample and presented as fold changes from the control.

4.17. Western blot analysis

Western blot analysis was performed as established protocol [45,46]. The primary antibodies used were as follows: anti-FAM3A (NBP2-75487, Novus), anti-NGAL (ab70287, abcam), anti-VDAC (#4661, CST), anti-NLRP3 (#15101, CST), anti-Caspase-1 (M025280 M, Abmart), anti-IL-18 (ab207323, abcam), anti-IL-1β (ab283818, abcam), anti-TOMM20 (ab186735, abcam), anti-GSDMD (ab219800, abcam; #69469, CST), anti-GSDME (ab215191, abcam), anti-p-PI3K (Tyr458, #4228, CST), anti-PI3K (#4292, CST), anti-AKT (#4685, CST), anti-*p*-AKT (Ser473, #4060, CST), anti-NRF2 (#12721, CST), anti-*p*-NRF2 (Ser40, ab76026, abcam), anti-TBP (#44059, CST), anti--α-tubulin (BM1452, Boster), anti-β-actin (BA2305, Boster), anti-GAPDH (BM1623, Boster).

4.18. Histology and immunohistochemical staining

Paraffin-embedded kidney sections (3 μm) were prepared in a routine procedure. Sections were stained with periodic acid-schiff (PAS, G1281, Solarbio) according to the manufacturer's instructions to identify injured tubules. Immunohistochemical staining was performed as established protocol. The antibodies used were as follows: anti-FAM3A (NBP2-75487, Novus), anti-Kim-1 (BA3537, Boster), anti-GSDMD-N (#36425, CST), anti-NLRP3 (#15101, CST), anti-p-PI3K (Tyr458, #4228, CST), anti-*p*-AKT (Ser473, #4060, CST), anti-*p*-NRF2 (Ser40, ab76026, abcam), anti-F4/80 (GB11027, Servicebio), anti-Ly6g (GB11229, Servicebio).

4.19. Quantifications of injured tubules

Kidney sections were stained with PAS and then ten high-powered (x400) fields were captured randomly from each section by microscope (Olympus, Japan). Criteria for quantifying injury tubules from renal sections were executed as described previously. The injury tubules were assessed by tubular dilation, hyaline casts, detached epithelial cells in tubular lumens, and detached brush borders. The ratio of injury tubules was calculated by three experienced observers in a blinded fashion.

4.20. Immunofluorescence staining

After dewaxing, hydrating and antigen retrieving, paraffin-embedded kidney sections were incubated with primary antibodies as follows: anti-E-cadherin (#3195, CST), anti-FAM3A (NBP2-75487, Novus), anti-TOMM20 (ab186735, abcam), anti-Lotus Tetragonolobus Lectin (LTL) (FL-1321; VECTOR Laboratories), anti-Peanut Agglutinin (PNA) (FL-1071; VECTOR Laboratories), anti-Dolichos Biflorus Agglutinin (DBA) (FL1031; VECTOR Laboratories).

For cell immunofluorescence staining, HKC-8 cells cultured on coverslips were fixed with cold 4% paraformaldehyde at room temperature for 15 min, followed by washing with PBS, blocking with 10% normal donkey serum, and incubating with primary antibodies as indicated.

4.21. qRT-PCR

qRT-PCR was performed as previously described [46–48]. Briefly, total RNA was extracted by using TRIzol RNA isolation system (Life Technologies, Grand Island, NY) according to the manufacturer's instruction. Then, 2 μg RNA was reverse-transcribed into cDNA using a PrimeScript RT reagent kit (R323-01, Vazyme, China), and RT-PCR was performed using SYBR Green PCR Master Mix (Q341-02, Vazyme, China) on a StepOnePlus Real-time PCR System (Applied Biosystems, USA). The primers used were listed in Table S1.

4.22. RNA sequencing and data analysis

The technology of transcriptome sequencing analysis was supported by Novogene (Beijing, China). The primary experimental procedures included total RNA extraction, qualification, quantification, library construction, clustering and sequencing, and final data analysis. The library quality was assessed on the Agilent Bioanalyzer 2100 system. Differential expression analysis was performed using the DESeq2 R package. Genes with an adjusted $P < 0.05$ were considered significantly differential expression. GO enrichment analysis of differentially expressed genes was performed using the cluster Profiler R package. GSEA analysis of different signaling pathways was performed based on the Molecular Signatures Database of GSEA web interface.

4.23. Single-cell RNA-seq data analysis

The technology of single-cell RNA-seq analysis was supported by Novogene (Beijing, China). Briefly, raw fastq files were obtained from previous studies [1,21] (Data include n = 2 sham, n = 6 IRI samples. Among these samples, sham-1, sham-2, IRI-1-1, IRI-1-2, IRI-3-1, IRI-3-2 data were obtained from GSE180420, IRI-1-3 and IRI-2-1 data obtained from GSE139506) and then were aligned to the mm10 (EnsemblGRCm38.93) reference genome and quantified using CellRanger. Seurat was used for data quality control according to the gene detected number, mitochondrial UMI ratio, etc. To ensure the reliability and accuracy of the subsequent analysis results, DoubletFinder was used for estimating doublets in scRNA-sequencing data and excluding the doublet-like cells. After excluding 5538 poor-quality cells, 33,518

singlet cells remained. For cell clustering, highly variable genes were selected and the principal component maps were constructed based on a list of marker genes [1], which was segmented with a resolution of 0.6. 14,150 tubular cells, including proximal straight tubule, proximal convoluted tubule, distal convoluted tubule, and loop of Henle, were used for further analysis. To identify different forms of programmed tubular cell death, markers for apoptosis (Casp3, Casp8, Bad, Bak1, Bax, Casp7, Bcap31, Bnip3, Ctsh, Ctsc, Dapk3, Mtch2, Ppp2r1a), pyroptosis (Casp1, Casp4, Pycard, Nlrp3, Aim2, Gsdmd, Gsdme, Il1b, Il18, Scaf11, Nod2, Naip2, Naip5), ferroptosis (Ptgs2, Chac2, Acsl4, Slc7a11, Hmox1, Trp53, Slc3a2, Map1lc3b, Trf, Cybb) and necroptosis (Fas, Fasl, Cflar, Ripk1, Chmp7, Hsp90aa1, Hsp90ab1) were used. Gene Ontology (GO) enrichment analysis of specific cell clusters was implemented using clusterProfiler R package, in which gene length bias was corrected. GO terms with corrected P value less than 0.05 were considered significantly enriched by marker gene. To compare gene expression between different samples, edgeR package was carried out to obtain zone-specific marker genes.

4.24. FAM3A network analysis

To identify the link between FAM3A and programmed cell death, network analysis was carried out. 53 FAM3A-related genes (Table S4) were extracted from previous studies and were used for network analysis. Among these genes, 7 genes were identified as the upstream signals of FAM3A, 29 genes were downstream signals of FMA3A and 17 genes were associated with the regulation of PI3K/AKT on cell death. Cytoscape and ClueGO were used to visualize the enriched biological processes associated with these genes.

4.25. Human genome Microarray analysis

The transcriptomics data of control kidney biopsies (n = 37), and the data of brain-dead kidney donors (n = 105) and cardiac-dead kidney donors (n = 64) after cold ischemia/reperfusion were obtained from previous study (GSE43974) [20]. The expression of FAM3A and pyroptosis-related genes and the correlation between FAM3A and pyroptosis were analyzed using Origin.

4.26. Statistical analyses

All data were expressed as mean ± standard error of the mean (SEM). Statistical analysis was performed using SPSS 19.0 (SPSS Inc, Chicago, USA). For comparisons between two groups, an unpaired two-tailed Student's t-test was used, and one-way analysis of variance (ANOVA) followed by the Least Significant Difference or Dunnett's T3 procedure for comparison of more than two groups. Bivariate correlation analysis was performed using Pearson and Spearman rank correlation analysis. The value of $P < 0.05$ was considered to be statistically significant.

CRediT authorship contribution statement

Xiaolong Li: Writing – original draft, Project administration, Investigation. **Feifei Yuan:** Project administration. **Yabing Xiong:** Project administration. **Ying Tang:** Project administration. **Zhiru Li:** Project administration. **Jun Ai:** Methodology. **Jinhua Miao:** Methodology. **Wenting Ye:** Methodology. **Shan Zhou:** Software. **Qinyu Wu:** Software. **Xiaoxu Wang:** Software. **Dan Xu:** Methodology. **Jiemei Li:** Software. **Jiewu Huang:** Visualization. **Qiurong Chen:** Software. **Weiwei Shen:** Visualization. **Youhua Liu:** Visualization. **Fan Fan Hou:** Visualization. **Lili Zhou:** Writing – review & editing, Writing – original draft, Funding acquisition, Formal analysis.

Declaration of competing interest

The authors declare that they have no competing interests.

Data availability

Data will be made available on request.

Acknowledgments

This work was supported by National Natural Science Foundation of China Grant 82225010, 82070707, 82200750, 82100786; and Outstanding Youths Development Scheme of Nanfang Hospital, Southern Medical University (2019J013, 2021J001) and the Presidential Foundation of Nanfang Hospital (Grant No. 2019Z006, 2021C023), and Guangdong Provincial Clinical Research Center for Kidney Disease (No. 2020B1111170013), and Guangdong Basic and Applied Basic Research Foundation (Grant No. 2021A1515110222).

Appendix A. Supplementary data

Supplementary data to this article can be found online at https://doi.org/10.1016/j.redox.2024.103225.

References

[1] M.S. Balzer, et al., Single-cell analysis highlights differences in druggable pathways underlying adaptive or fibrotic kidney regeneration, Nat. Commun. 13 (2022) 4018, https://doi.org/10.1038/s41467-022-31772-9.
[2] K.J. Jager, et al., A single number for advocacy and communication-worldwide more than 850 million individuals have kidney diseases, Kidney Int. 96 (2019) 1048–1050, https://doi.org/10.1016/j.kint.2019.07.012.
[3] J.A. Kellum, et al., Acute kidney injury, Nat Rev Dis Primers 7 (2021) 52, https://doi.org/10.1038/s41572-021-00284-z.
[4] A.B. Sanz, M.D. Sanchez-Nino, A.M. Ramos, A. Ortiz, Regulated cell death pathways in kidney disease, Nat. Rev. Nephrol. 19 (2023) 281–299, https://doi.org/10.1038/s41581-023-00694-0.
[5] E.E. Elias, B. Lyons, D.A. Muruve, Gasdermins and pyroptosis in the kidney, Nat. Rev. Nephrol. 19 (2023) 337–350, https://doi.org/10.1038/s41581-022-00662-0.
[6] C.G. Hsu, et al., The lipid peroxidation product 4-hydroxynonenal inhibits NLRP3 inflammasome activation and macrophage pyroptosis, Cell Death Differ. 29 (2022) 1790–1803, https://doi.org/10.1038/s41418-022-00966-5.
[7] P. Yu, et al., Pyroptosis: mechanisms and diseases, Signal Transduct Target Ther 6 (2021) 128, https://doi.org/10.1038/s41392-021-00507-5.
[8] S.R. Mulay, Multifactorial functions of the inflammasome component NLRP3 in pathogenesis of chronic kidney diseases, Kidney Int. 96 (2019) 58–66, https://doi.org/10.1016/j.kint.2019.01.014.
[9] W. Tonnus, et al., The clinical relevance of necroinflammation-highlighting the importance of acute kidney injury and the adrenal glands, Cell Death Differ. 26 (2019) 68–82, https://doi.org/10.1038/s41418-018-0193-5.
[10] L. Su, J. Zhang, H. Gomez, J.A. Kellum, Z. Peng, Mitochondria ROS and mitophagy in acute kidney injury, Autophagy 19 (2023) 401–414, https://doi.org/10.1080/15548627.2022.2084862.
[11] C. Tang, et al., Mitochondrial quality control in kidney injury and repair, Nat. Rev. Nephrol. 17 (2021) 299–318, https://doi.org/10.1038/s41581-020-00369-0.
[12] X. Zhang, et al., FAM3 gene family: a promising therapeutical target for NAFLD and type 2 diabetes, Metabolism 81 (2018) 71–82, https://doi.org/10.1016/j.metabol.2017.12.001.
[13] H. Yan, et al., FAM3A maintains metabolic homeostasis by interacting with F1-ATP synthase to regulate the activity and assembly of ATP synthase, Metabolism 139 (2023) 155372, https://doi.org/10.1016/j.metabol.2022.155372.
[14] C. Wang, et al., FAM3A activates PI3K p110alpha/Akt signaling to ameliorate hepatic gluconeogenesis and lipogenesis, Hepatology 59 (2014) 1779–1790, https://doi.org/10.1002/hep.26945.
[15] R. Xiang, et al., VSMC-specific deletion of FAM3A attenuated Ang II-promoted Hypertension and Cardiovascular Hypertrophy, Circ. Res. 126 (2020) 1746–1759, https://doi.org/10.1161/CIRCRESAHA.119.315558.
[16] W. Xu, M. Liang, Y. Zhang, K. Huang, C. Wang, Endothelial FAM3A positively regulates post-ischaemic angiogenesis, EBioMedicine 43 (2019) 32–42, https://doi.org/10.1016/j.ebiom.2019.03.038.
[17] S. Jia, et al., FAM3A promotes vascular smooth muscle cell proliferation and migration and exacerbates neointima formation in rat artery after balloon injury, J. Mol. Cell. Cardiol. 74 (2014) 173–182, https://doi.org/10.1016/j.yjmcc.2014.05.011.
[18] Q. Song, et al., FAM3A ameliorates brain impairment induced by hypoxia-ischemia in Neonatal rat, Cell. Mol. Neurobiol. (2021), https://doi.org/10.1007/s10571-021-01172-6.
[19] X. Liu, et al., Imipramine activates FAM3A-FOXA2-CPT2 pathway to ameliorate hepatic steatosis, Metabolism 136 (2022) 155292, https://doi.org/10.1016/j.metabol.2022.155292.
[20] J. Damman, et al., Hypoxia and Complement-and-Coagulation pathways in the Deceased organ donor as the major target for Intervention to improve renal

Allograft Outcome, Transplantation 99 (2015) 1293–1300, https://doi.org/10.1097/TP.0000000000000500.
[21] V. Rudman-Melnick, et al., Single-cell Profiling of AKI in a murine model reveals novel transcriptional Signatures, Profibrotic phenotype, and epithelial-to-Stromal Crosstalk, J. Am. Soc. Nephrol. 31 (2020) 2793–2814, https://doi.org/10.1681/ASN.2020010052.
[22] F. Maremonti, C. Meyer, A. Linkermann, Mechanisms and models of kidney tubular Necrosis and nephron loss, J. Am. Soc. Nephrol. 33 (2022) 472–486, https://doi.org/10.1681/ASN.2021101293.
[23] Z. Zhu, et al., Transition of acute kidney injury to chronic kidney disease: role of metabolic reprogramming, Metabolism 131 (2022) 155194, https://doi.org/10.1016/j.metabol.2022.155194.
[24] S. Kumar, Cellular and molecular pathways of renal repair after acute kidney injury, Kidney Int. 93 (2018) 27–40, https://doi.org/10.1016/j.kint.2017.07.030.
[25] M. Guerrero-Hue, et al., Curcumin reduces renal damage associated with rhabdomyolysis by decreasing ferroptosis-mediated cell death, FASEB J 33 (2019) 8961–8975, https://doi.org/10.1096/fj.201900077R.
[26] S.J. Song, et al., Rhabdomyolysis-induced AKI was ameliorated in NLRP3 KO mice via alleviation of mitochondrial lipid peroxidation in renal tubular cells, Int. J. Mol. Sci. 21 (2020), https://doi.org/10.3390/ijms21228564.
[27] Q. Lin, et al., Inhibiting NLRP3 inflammasome attenuates apoptosis in contrast-induced acute kidney injury through the upregulation of HIF1A and BNIP3-mediated mitophagy, Autophagy 17 (2021) 2975–2990, https://doi.org/10.1080/15548627.2020.1848971.
[28] N. Miao, et al., The cleavage of gasdermin D by caspase-11 promotes tubular epithelial cell pyroptosis and urinary IL-18 excretion in acute kidney injury, Kidney Int. 96 (2019) 1105–1120, https://doi.org/10.1016/j.kint.2019.04.035.
[29] X. Liu, et al., Mitochondrial calpain-1 activates NLRP3 inflammasome by cleaving ATP5A1 and inducing mitochondrial ROS in CVB3-induced myocarditis, Basic Res. Cardiol. 117 (2022) 40, https://doi.org/10.1007/s00395-022-00948-1.
[30] C.G. Weindel, et al., Mitochondrial ROS promotes susceptibility to infection via gasdermin D-mediated necroptosis, Cell 185 (2022) 3214–3231 e3223, https://doi.org/10.1016/j.cell.2022.06.038.
[31] J. Liu, et al., Mechanism of Snhg8/miR-384/Hoxa13/FAM3A axis regulating neuronal apoptosis in ischemic mice model, Cell Death Dis. 10 (2019) 441, https://doi.org/10.1038/s41419-019-1631-0.
[32] S. Yan, C. Jiang, H. Li, D. Li, W. Dong, FAM3A protects chondrocytes against interleukin-1beta-induced apoptosis through regulating PI3K/Akt/mTOR pathway, Biochem. Biophys. Res. Commun. 516 (2019) 209–214, https://doi.org/10.1016/j.bbrc.2019.06.016.
[33] N. El Mjiyad, A. Caro-Maldonado, S. Ramirez-Peinado, C. Munoz-Pinedo, Sugar-free approaches to cancer cell killing, Oncogene 30 (2011) 253–264, https://doi.org/10.1038/onc.2010.466.
[34] A. Lin, et al., The FoxO-BNIP3 axis exerts a unique regulation of mTORC1 and cell survival under energy stress, Oncogene 33 (2014) 3183–3194, https://doi.org/10.1038/onc.2013.273.
[35] H. Lee, et al., Energy-stress-mediated AMPK activation inhibits ferroptosis, Nat. Cell Biol. 22 (2020) 225–234, https://doi.org/10.1038/s41556-020-0461-8.
[36] Y. Li, et al., The DNA repair Nuclease MRE11A functions as a mitochondrial protector and Prevents T cell pyroptosis and tissue inflammation, Cell Metab 30 (2019) 477–492 e476, https://doi.org/10.1016/j.cmet.2019.06.016.
[37] D. Sala, et al., The Stat3-Fam3a axis promotes muscle stem cell myogenic lineage progression by inducing mitochondrial respiration, Nat. Commun. 10 (2019) 1796, https://doi.org/10.1038/s41467-019-09746-1.
[38] V. Vallon, R. Unwin, E.W. Inscho, J. Leipziger, B.K. Kishore, Extracellular Nucleotides and P2 receptors in renal function, Physiol. Rev. 100 (2020) 211–269, https://doi.org/10.1152/physrev.00038.2018.
[39] L. Fao, S.I. Mota, A.C. Rego, Shaping the Nrf2-ARE-related pathways in Alzheimer's and Parkinson's diseases, Ageing Res. Rev. 54 (2019) 100942, https://doi.org/10.1016/j.arr.2019.100942.
[40] Y. Mitsuishi, et al., Nrf2 redirects glucose and glutamine into anabolic pathways in metabolic reprogramming, Cancer Cell 22 (2012) 66–79, https://doi.org/10.1016/j.ccr.2012.05.016.
[41] S. Liao, et al., A novel compound DBZ ameliorates neuroinflammation in LPS-stimulated microglia and ischemic stroke rats: role of Akt(Ser473)/GSK3beta (Ser9)-mediated Nrf2 activation, Redox Biol. 36 (2020) 101644, https://doi.org/10.1016/j.redox.2020.101644.
[42] Y. Li, et al., GSDME-mediated pyroptosis promotes inflammation and fibrosis in obstructive nephropathy, Cell Death Differ. 28 (2021) 2333–2350, https://doi.org/10.1038/s41418-021-00755-6.
[43] S. Chen, et al., Tenascin-C protects against acute kidney injury by recruiting Wnt ligands, Kidney Int. 95 (2019) 62–74, https://doi.org/10.1016/j.kint.2018.08.029.
[44] D. Zhou, et al., Matrix Metalloproteinase-7 is a urinary Biomarker and pathogenic mediator of kidney fibrosis, J. Am. Soc. Nephrol. 28 (2017) 598–611, https://doi.org/10.1681/ASN.2016030354.
[45] S. Zhou, et al., Cannabinoid receptor type 2 promotes kidney fibrosis through orchestrating beta-catenin signaling, Kidney Int. 99 (2021) 364–381, https://doi.org/10.1016/j.kint.2020.09.025.
[46] X.L. Li, et al., Blockade of TMEM16A protects against renal fibrosis by reducing intracellular Cl(-) concentration, Br. J. Pharmacol. 179 (2022) 3043–3060, https://doi.org/10.1111/bph.15786.
[47] S. Chen, et al., beta-catenin-controlled tubular cell-derived exosomes play a key role in fibroblast activation via the OPN-CD44 axis, J. Extracell. Vesicles 11 (2022) e12203, https://doi.org/10.1002/jev2.12203.
[48] J. Li, et al., B7-1 mediates podocyte injury and glomerulosclerosis through communication with Hsp90ab1-LRP5-beta-catenin pathway, Cell Death Differ. (2022), https://doi.org/10.1038/s41418-022-01026-8.